ANALYSIS OF SLOT COUPLED MICROSTRIP PATCH ANTENNAS

A THESIS SUBMITTED TO
THE GRADUATE SCHOOL OF NATURAL AND APPLIED SCIENCES
OF
MIDDLE EAST TECHNICAL UNIVERSITY

BY

ELİF BALLIKAYA

IN PARTIAL FULFILLMENT OF THE REQUIREMENTS
FOR
THE DEGREE OF MASTER OF SCIENCE
IN
ELECTRICAL AND ELECTRONICS ENGINEERING

DECEMBER 2007

ANALYSIS OF SLOT COUPLED MICROSTRIP PATCH ANTENNAS

submitted by **ELİF BALLIKAYA** in partial fulfillment of the requirements for the degree of **Master of Science in Electrical and Electronics Engineering Department, Middle East Technical University** by,

Prof. Dr. Canan Özgen, _____
Dean, Graduate School of **Natural and Applied Sciences**

Prof. Dr. İsmet Erkmen _____
Head of Department, **Electrical and Electronics Engineering**

Assoc. Prof. Dr. Özlem Aydın Çivi _____
Supervisor, **Electrical and Electronics Engineering Dept., METU**

Examining Committee Members:

Prof. Dr. Mustafa Kuzuoğlu _____
Electrical and Electronics Engineering Dept., METU

Assoc. Prof. Dr. Özlem Aydın Çivi _____
Electrical and Electronics Engineering Dept., METU

Prof. Dr. Gülbin Dural _____
Electrical and Electronics Engineering Dept., METU

Assist. Prof. Dr. Lale Alatan _____
Electrical and Electronics Engineering Dept., METU

Assoc. Prof. Dr. Vakur B. Ertürk _____
Electrical and Electronics Engineering Dept., Bilkent U.

Date: 07.12.2007

I hereby declare that all information in this document has been obtained and presented in accordence with academic rules and ethical conduct. I also declare that, as required by these rules and conduct, I have fully cited and referenced all material and results that are not original to this work.

Name, Last name : Elif Ballıkaya

Signature :

ABSTRACT

ANALYSIS OF SLOT COUPLED MICROSTRIP PATCH ANTENNAS

Ballıkaya, Elif

M.Sc., Department of Electrical and Electronics Engineering

Supervisor : Assoc.Prof.Dr. Özlem Aydın Çivi

December 2007, 61 pages

Method of Moments (MoM)/Green's function formulation is developed for the analysis of electromagnetic radiation from planar rectangular microstrip antennas with different feeding techniques. Investigated structures are microstrip line fed patch antenna, proximity coupled patch antenna and slot coupled patch antenna. For all these structures equivalent problems are defined. Then, integral equations where currents are the unknowns are obtained from boundary conditions and by using spectral domain representation of Green's functions. Finally, MoM is applied to convert these integral equations to a system of linear equations. Currents on the conducting surfaces as well as equivalent magnetic currents on the apertures are modeled as a sum of piecewise sinusoidal subdomain basis functions with unknown coefficients which are calculated by solving the system of linear equations. Based on the formulations provided in this study, a Fortran code is developed. Numerical results calculated by using the code are presented in the form of patch and line currents and input impedances. Presented results are in good agreement with the results given in the literature.

Keywords: Microstrip Antennas, Spectral Domain Green's Functions, Method of Moments

ÖZ

AÇIKLIK KUPLAJLI MİKROŞERİT YAMA ANTEN ANALİZİ

Ballıkaya, Elif

Yüksek Lisans, Elektrik ve Elektronik Mühendisliği Bölümü

Tez Yöneticisi : Doç. Dr. Özlem Aydın Çivi

Aralık 2007, 61 sayfa

Bu tez çalışmasında farklı tekniklerle beslenen dikdörtgen mikroşerit yama antenlerin analizi için Moment Metodu/Green's fonksiyonu formulasyonu geliştirilmiştir. İncelenen yapılar mikroşerit hat ile beslenen yama anten, yakınlık kuplajlı yama anten ve açıklık kuplajlı yama antendir. Bütün antenler için denk yapılar tanımlanmıştır. Sonrasında sınır koşulları ve spektral Green fonksiyonları kullanılarak, akımların bilinmeyen olarak tanımlandığı integral denklemler elde edilmiştir. Son olarak bu integral denklemlerin doğrusal denklem sistemine dönüştürülmesi için moment metodu kullanılmıştır. İletken yüzeyler üzerindeki elektrik akımlar ve açıklıklarda tanımlanan eşdeğer manyetik akımlar, parçalı sinüs temel fonksiyonları ve bilinmeyen katsayılar cinsinden yazılmıştır. Akımların temel fonksiyonlarla açılımdaki bu bilinmeyen katsayılar doğrusal denklem sisteminin çözümünden elde edilmiştir. Bu tezde sunulan formulasyonu uygulayan bir Fortran kodu geliştirilmiştir. Mikroşerit hat ve yama üzerindeki akım dağılımları ve antenin giriş empedansları bu kodun kullanımıyla elde edilen edilmiş ve sunulmuştur. Elde edilen sonuçların literatürdeki sonuçlarla uyumlu olduğu görülmüştür.

Anahtar Kelimeler: Mikroşerit Antenler, Spektral Uzam Green Fonksiyonları, Moment Metodu

TABLE OF CONTENTS

CHAPTER 1

INTRODUCTION

In this thesis, planar rectangular microstrip patch antennas fed by different techniques are analyzed using Method of Moments/Spectral Domain Green's function method. Specifically, formulations for the analysis of radiation from microstrip line fed, proximity coupled and slot coupled microstrip patch antennas are provided. Numerical results in the form of current distributions and input impedance are presented and compared with the results given in literature.

A microstrip antenna idea was firstly introduced in 1950's but it became popular and took place in various applications in 1970's. Recently, microstrip antennas are widely used in several applications where low size, weight and cost, high performance and easily fabricated and installed antennas are required such as airborne, space borne commercial and military applications and mobile and wireless technologies. Some other advantages of microstrip antennas are that they are conformable to planar and non-planar surfaces, easily fabricated using printed circuit technology, and they are mechanically robust. Microstrip patches are resonant type antennas. Thus, impedance bandwidths are narrow. The other disadvantages of microstrip antennas are having low efficiency, low power handling, and spurious feed radiation.

A microstrip patch antenna consists of a radiating conducting strip placed on a grounded dielectric layer. Design of the radiating patch (length, width, feed type etc.)

and characteristic of the dielectric substrate (dielectric constant, height of the substrate etc.) determines the behavior of the antenna. Microstrip patch can be of different shapes such as rectangular, square or disk patches. They can provide linear, dual or circular polarization by appropriate feeding.

Experimental studies on the design of microstrip antennas have shown that most effective parameter on the characteristic of a microstrip antenna is the dielectric constant of the substrate. Relation between dielectric constant and the resonance frequency of a microstrip antenna can be written as

$$\frac{\delta f}{f_r} = -\frac{1}{2}\frac{\delta \varepsilon_r}{\varepsilon_r} \tag{1.1}$$

f_r is the resonant frequency, δf is the change in resonance frequency, $\delta \varepsilon_r$ is the change in dielectric constant and ε_r is the dielectric constant of the substrate, [1]. Change in the size of the patch results in a change in the resonance frequency where

$$\frac{\delta f}{f_r} = -\frac{\delta W}{W} \tag{1.2}$$

δW is the change in patch width, W is the patch width. W is usually chosen in the range $\lambda_0/3 < W < \lambda_0/2$. Ratio of $L/W > 2$ is not advised. L is the patch length, [1].

Thickness of the dielectric substrate is less effective on the resonance frequency compared to dielectric constant. $0.003\lambda_0 \leq h \leq 0.1\lambda_0$ is generally used. Substrate material used in today's technology has a dielectric constant that varies from 1.17 to 25. Usually small dielectric constant materials are preferred since they supply better efficiency, larger bandwidth with thick substrates but large patches.

Due to the change of dielectric constant, total resonance frequency change between -75^0C and 100^0C is generally about %0.03 which means it is nearly possible to

eliminate the effect of temperature on the resonance frequency of a microstrip antenna if a proper material is selected, [1].

Different feeding techniques of microstrip patch antennas are shown in Figure 1.1. Microstrip line and coaxial probe feed methods, shown in Figure 1.1.a and Figure 1.1.b, are advantageous because of their simplicity to match and fabricate but they are both bandwidth limited when substrate thickness is increased. It is also difficult to model a probe fed microstrip antenna with a thick substrate. Also unwanted feed radiation in these feed types interferes with the radiation of the patch.

To overcome the problems of microstrip line and coaxial probe feeds, noncontacting feed methods are developed. In proximity coupled microstrip antenna, shown in Figure 1.1.c, two dielectric layers are separated by a microstrip line. Radiating patch is located at the top of the upper dielectric layer while lower dielectric layer is bounded by a ground plane. Of the four feeds shown in Figure 1.1, proximity coupling is the method that provides the largest bandwidth. Spurious feed radiation is reduced by removing the direct contact between the feed and patch.

Slot coupled microstrip patch antenna, shown in Figure 1.1.d is proposed by Pozar in 1985, [2]. It is also a noncontacting feed method. The structure consists of two dielectric layers, which may have different thickness and dielectric constants. These two layers are separated by a ground plane with a slot, which provides coupling between the patch and the feed line. The upper dielectric layer is bounded from top by a radiating patch where the lower dielectric layer is bounded from bottom by the feed network. Feed network, shape of the patch and parameters of the dielectric substrates can be designed separately to obtain a desired performance from the antenna. One can choose thick dielectric with low dielectric constant for the patch to increase operation bandwidth and choose thin dielectric with high dielectric constant for the feed network. Since feed network part and radiating part are separated from each other, aperture coupled patch is very suitable for phased arrays [2], [3].

After Pozar introduced this new and advantageous feed technique a number of studies have been carried out to analyze it. Pozar analyzed this structure using cavity model and also gave results obtained from the measurement of a prototype antenna. Modal expansion method is also applied to slot coupled microstrip antennas in [4]. Input impedance calculation of slot coupled microstrip antennas using transmission line modeling is presented in [5], [6]. They also show good agreement with the measured results. Thirdly, moment method analysis of this antenna is explained in detail in [7]. To improve the antenna performance by improving the coupling between the patch and feed line, different size and shapes of slots are experimented. H-shaped, bowtie, dog bone shaped slots had been studied [8], [9]. All these slot shapes provide better input impedance compared to a rectangular slot. They also have smaller dimensions compared to rectangular slot, which decreases the amount of back radiation through the aperture. Only disadvantage of these complicated slot geometries is that it is difficult to analyze these structures analytically or even numerically. Besides slot shape, patch and feed shapes are also varied to design a wideband microstrip antenna. Some different shapes of patch and feed, like T-shaped feed, are presented in [10]. Furthermore the effects of dielectric constants of the layers are investigated, [11], [3]. Studies have shown that it is advantageous to choose a high dielectric constant material for the lower substrate (for feed) and a thick and low dielectric constant material for the upper substrate (for patch).

In the analysis of radiation/scattering from microstrip patch antennas, full-wave analysis method, Method of Moments (MoM) is widely used, [12]. In this thesis MoM/Green's function technique in Spectral domain is used to investigate some microstrip patch antenna structures. In Chapter 2, some of the well-known methods used to analyze microstrip antennas are summarized. These are transmission line method, cavity method and full-wave numerical methods such as MoM.

In Chapter 3, Green's function representation in spectral domain is presented for electric and magnetic type sources located on grounded dielectric substrate.

Formulations for microstrip line, microstrip line fed patch, proximity coupled patch and slot coupled patch antennas are derived and given in Chapter 3. For all these cases equivalent problems are defined and integral equations are obtained from boundary conditions. Then, MoM is applied to convert these integral equations to a system of linear equations. Currents on the conducting surfaces as well as equivalent magnetic currents on the apertures are modeled as a sum of piecewise sinusoidal sub domain basis functions with unknown coefficients which are calculated by solving the system linear equations. Accurate and efficient evaluation of MoM matrix entities are discussed in Chapter 3. Calculation of input impedance of a patch antenna is also explained.

Numerical results in the form of line and patch currents and input impedance are obtained by using formulations derived in Chapter 3. These numerical results in comparison with the available data in the literature are presented and discussed in Chapter 4.

Chapter 5 concludes this thesis and briefly discusses the work done in this thesis. An $e^{j\omega t}$ time dependence is assumed and suppressed throughout this work.

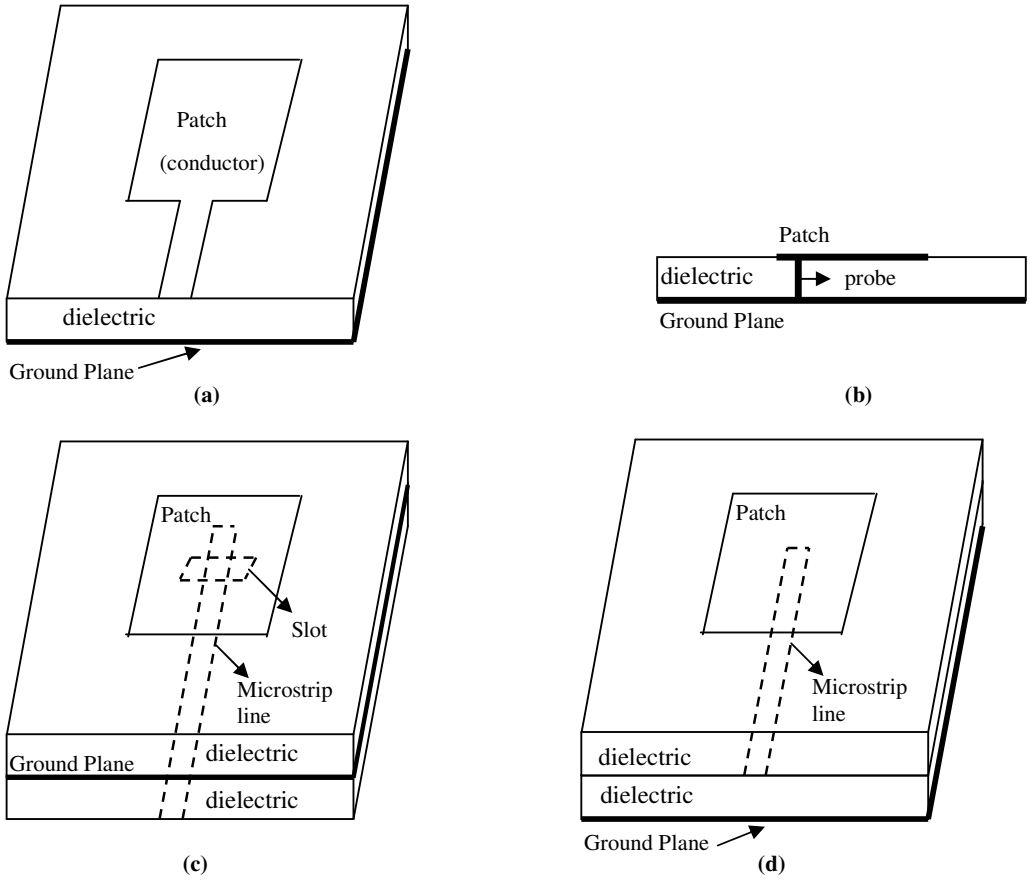

Figure 1.1 – (a) Microstrip line fed (b) Coaxial probe fed (c) Slot coupled (d) Proximity coupled microstrip antenna

CHAPTER 2

METHODS OF ANALYSIS OF MICROSTRIP ANTENNAS

Recently, microstrip antennas are preferred in many commercial and military applications, due to their several advantages, such as low profile, low cost, easy integration. Therefore, there is a significant effort on the development of efficient and accurate analysis tools for microstrip antennas. Microstrip antennas are generally analyzed by three different models. These are transmission line model, cavity model and full-wave numerical methods such as Method of Moments. In the transmission line method, microstrip antenna is represented by an equivalent circuit and characteristic impedance and propagation constant are expressed in closed form. Cavity model is a modal solution and it gives field distributions in the cavity between microstrip patch and the ground plane surrounded by magnetic walls. Application of these two methods is limited due to approximations made. To obtain more accurate results full-wave numerical methods, such as Method of Moments, Finite Element, Finite Difference Time Domain, are preferred. In this thesis, Method of Moments is chosen to investigate patch antennas, since it can be easily applied to planar antenna structures and solution time is relatively short compared to other mentioned numerical methods.

2.1 Transmission Line Model

The simplest and the least accurate method to analyze a rectangular microstrip patch is the transmission line method. It basically represents the antenna by two parallel

radiating slots separated by a transmission line of length L, which is equal to the length of the patch, and characteristic impedance Z_c. Transmission line representation of a microstrip patch antenna is shown in Figure 2.1. The slot length is equal to the width of the patch and the slot width is equal to the thickness of the substrate.

Fields at the edge of the patch, both for the length and the width, undergo fringing as a result of the finite dimension of the patch. Besides the dimensions, height and dielectric constant of the substrate also affect the amount of fringing. Because of fringing, patch looks wider then its physical dimensions. In order to take in to account this effect, an effective dielectric constant ε_{reff} is calculated as [3]:

$$W/h > 1$$
$$\varepsilon_{reff} = \frac{\varepsilon_r + 1}{2} + \frac{\varepsilon_r - 1}{2}\left[1 + 10\frac{h}{W}\right]^{-1/2} \tag{2.1}$$

where W is the patch width (slot length), h is the height of substrate (slot width) and ε_r is the dielectric constant of the substrate. Similarly effective patch length can be written in terms of effective dielectric constant as:

$$\frac{\Delta L}{h} = 0.412\frac{\left(\varepsilon_{reff} + 0.3\right)\left(\frac{W}{h} + 0.264\right)}{\left(\varepsilon_{reff} - 0.258\right)\left(\frac{W}{h} + 0.8\right)} \tag{2.2}$$
$$L_{eff} = L + 2\Delta L$$

Without fringing resonant frequency of the antenna is formulated as

$$f_r = \frac{1}{2L\sqrt{\varepsilon_r}\sqrt{\mu_0\varepsilon_0}} = \frac{v_0}{2L\sqrt{\varepsilon_r}} \tag{2.3}$$

where v_0 is the speed of light in free space. In order to take into account fringing, effective patch length and effective dielectric constant are used to formulate resonant frequency.

$$f_{rc} = \frac{1}{2L_{eff}\sqrt{\varepsilon_{reff}}\sqrt{\mu_0\varepsilon_0}} = \frac{1}{2(L+2\Delta L)\sqrt{\varepsilon_{reff}}\sqrt{\mu_0\varepsilon_0}}$$
$$= q\frac{1}{2L\sqrt{\varepsilon_r}\sqrt{\mu_0\varepsilon_0}} = q\frac{v_0}{2L\sqrt{\varepsilon_r}} \tag{2.4}$$

q in (2.4) is called the fringing factor and assumed as constant for other parameters of antenna when dielectric constant of the substrate and the frequency are not changed. Accuracy of the resonant frequency is defined by fringing factor.

As mentioned earlier, equivalent circuit of radiating slots used to represent microstrip patch consists of equivalent parallel admittance Y with conductance G and susceptance B. Related circuit and fringing is shown in Figure 2.1. Y can be written as [3]

$$Y = G + jB$$
$$G = \frac{W}{120\lambda_0}\left[1 - \frac{1}{24}(k_0 h)^2\right] \qquad \frac{h}{\lambda_0} < \frac{1}{10} \tag{2.5}$$
$$B = \frac{W}{120\lambda_0}\left[1 - 0.636\ln(k_0 h)^2\right] \qquad \frac{h}{\lambda_0} < \frac{1}{10}$$

where λ_0 is free space wavelength and $k_0 = 2\pi/\lambda_0$ is the free space wave number.

Since the slots are identical, (2.5) is valid for both of the slots.

Ideally, λ/2 separation between slots provides 180^0 phase difference, where λ is the wavelength in the substrate, but because of fringing, separation between the slots is slightly less then λ/2. So L is chosen properly in the range 0.48 λ<*L*<0.49 λ which results the admittance in slot 2 as

$$\tilde{Y}_2 = \tilde{G}_2 + j\tilde{B}_2 = G_1 - jB_1$$
$$\tilde{G}_2 = G_1 \tag{2.6}$$
$$\tilde{B}_2 = -B_1$$

Parallel admittances generates a pure real total resonant input admittance

$$\begin{aligned} Y_{in} &= G_1 + jB_1 + \tilde{G}_2 + j\tilde{B}_2 \\ &= G_1 + jB_1 + G_1 - jB_1 \\ &= 2G_1 \end{aligned} \tag{2.7}$$

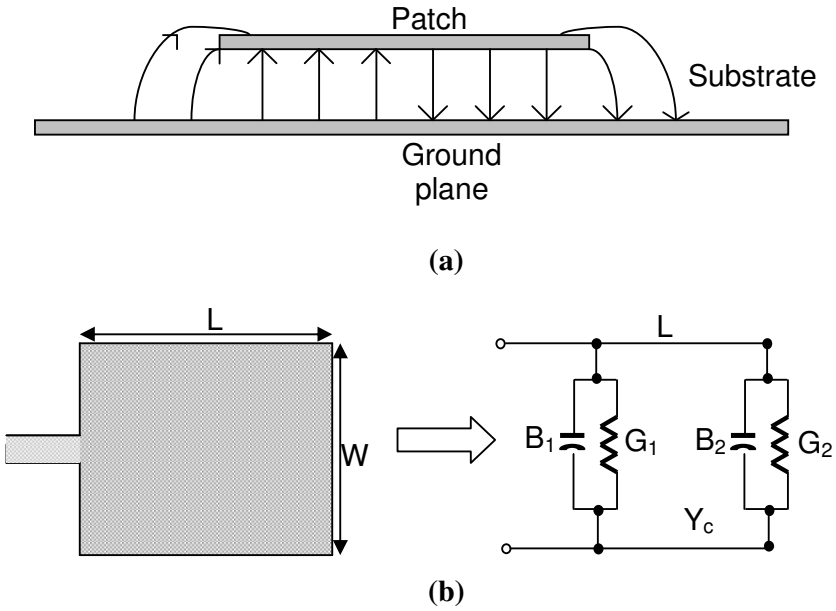

Figure 2.1 – (a) Fringing effect (b) Transmission line model of rectangular microstrip antenna

Although transmission line model provides less accuracy, calculation of resonant frequency and input admittance of a microstrip antenna is simple by this method.

The transmission line model is improved to calculate the input impedance of a slot coupled microstrip antenna. Equivalent transmission line model circuit of a slot coupled microstrip antenna is shown in Figure 2.2. First transformer stands for the coupling between the slot and patch while the second transformer is used to represent coupling between slot and microstrip line. Although derivation will not be formulated here, calculated input impedance is given in [5] as

$$Z_{in} = \frac{n_2^2}{\left(n_1^2 Y_{patch} + Y_{ap}\right)} - jZ_c \cot(k_l L_s) \tag{2.8}$$

where

$n_1 = L_a / b$

$n_2 = \Delta V / V_0$

k_l : wave number of microstrip line of length L_s

Z_c : characteristic impedance of microstrip line of length L_s

L_a : slot length

b: patch length

ΔV : discontinuity in modal voltage of feeding microstrip line

V_0: slot voltage

Detailed explanation about transmission line model of slot coupled microstrip antenna is provided in [5], [6].

2.2 Cavity Model

Another method used to analyze microstrip antennas is cavity method. Cavity model treats the region between the patch and the ground plane as a cavity bounded by these conductors from the top and the bottom and by magnetic walls along the perimeter of the patch in order to simulate an open circuit. It assumes that fields in

the cavity do not exceed the boundaries of the cavity which means fringing is not taken into account in the cavity model [3].

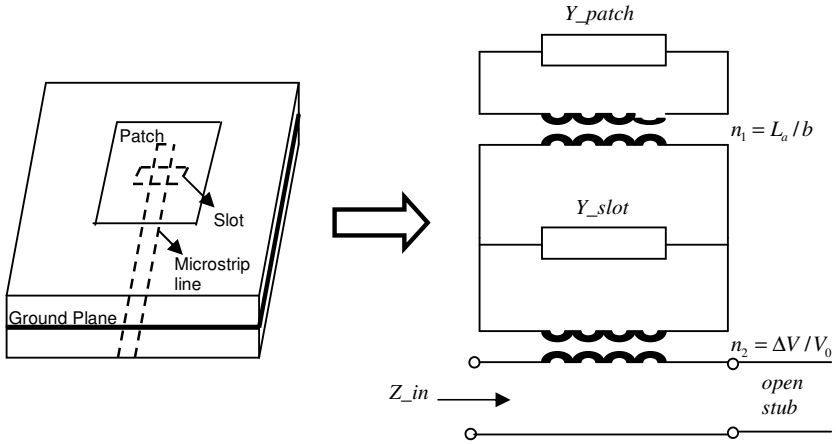

Figure 2.2 – Transmission line model of slot coupled microstrip antenna

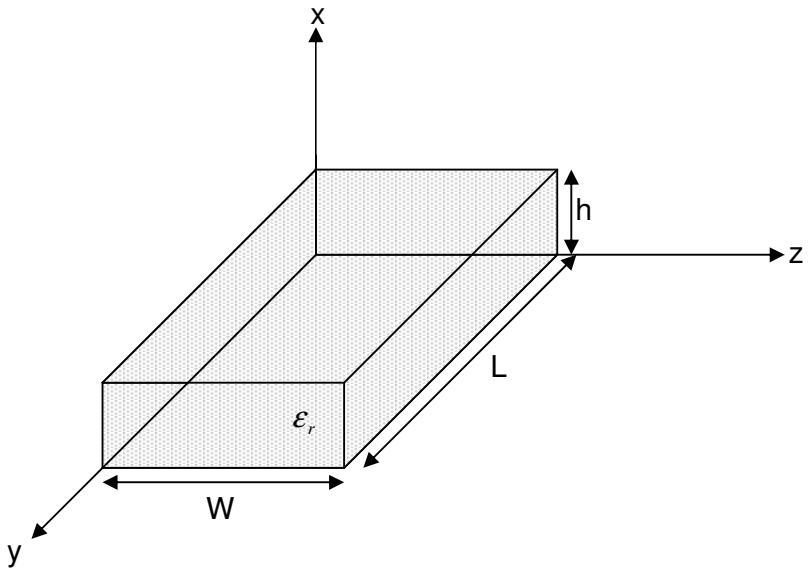

Figure 2.3 - Rectangular patch geometry

Under this assumption, electric and magnetic fields inside the cavity must satisfy the boundary conditions in (2.9) for a geometry shown in Figure 2.3.

$$\begin{aligned} &E_y(x'=0,0\le y'\le L,0\le z'\le W)=E_y(x'=h,0\le y'\le L,0\le z'\le W)=0\\ &H_y(0\le x'\le h,0\le y'\le L,z'=0)=H_y(0\le x'\le h,0\le y'\le L,z'=W)=0\\ &H_z(0\le x'\le h,y'=0,0\le z'\le W)=H_z(0\le x'\le h,y'=L,0\le z'\le W)=0 \end{aligned} \tag{2.9}$$

These fields can be written in terms of a vector potential A as

$$\begin{aligned} E_x &= -j\frac{1}{\omega\mu\varepsilon}\left(\frac{\partial^2}{\partial x^2}+k^2\right)A_x \qquad H_x = 0\\ E_y &= -j\frac{1}{\omega\mu\varepsilon}\frac{\partial^2 A_x}{\partial x\partial y} \qquad H_y = \frac{1}{\mu}\frac{\partial A_x}{\partial z}\\ E_z &= -j\frac{1}{\omega\mu\varepsilon}\frac{\partial^2 A_x}{\partial x\partial z} \qquad H_z = -\frac{1}{\mu}\frac{\partial A_x}{\partial y} \end{aligned} \tag{2.10}$$

where A satisfies the homogeneous wave equation

$$\nabla^2 A_x + k^2 A_x = 0 \tag{2.11}$$

Solution of A is

$$A_x = \left(A_1\cos(k_x x)+B_1\sin(k_x x)\right)\left(A_2\cos(k_y y)+B_2\sin(k_y y)\right)\left(A_3\cos(k_z z)+B_3\sin(k_z z)\right) \tag{2.12}$$

Inserting (2.12) into (2.10), one can show using the boundary condition for E_y that [3]

$$B_1 = 0, \qquad k_x = \frac{m\pi}{h}, \qquad m = 0,1,2... \tag{2.13}$$

Similarly, for the boundary condition for H_y

$$B_3 = 0, \quad k_z = \frac{p\pi}{W}, \quad p = 0,1,2... \tag{2.14}$$

and for H_z

$$B_2 = 0, \quad k_y = \frac{n\pi}{L}, \quad n = 0,1,2... \tag{2.15}$$

Resonant frequency of the cavity is

$$f_{r,mnp} = \frac{1}{2\pi\sqrt{\mu\varepsilon}}\sqrt{\left(\frac{m\pi}{h}\right)^2 + \left(\frac{n\pi}{L}\right)^2 + \left(\frac{p\pi}{W}\right)^2} \tag{2.16}$$

Dominant mode is the mode with the lowest order resonant frequency. For a microstrip antenna that satisfy $L>W>h$, TM_{010} is the dominant mode and resonant frequency is

$$f_{r,010} = \frac{1}{2L\sqrt{\mu\varepsilon}} \tag{2.17}$$

If microstrip antenna satisfies $L>W>L/2>h$ second order mode is TM_{001} and resonant frequency is

$$f_{r,001} = \frac{1}{2W\sqrt{\mu\varepsilon}} \tag{2.18}$$

If $L>L/2>W>h$ is valid, then the second order mode is TM_{020} and resonant frequency is

$$f_{r,020} = \frac{1}{L\sqrt{\mu\varepsilon}} \tag{2.19}$$

Cavity model is also limited; it is not possible to analyze a circular patch by using transmission line model. Furthermore, it ignores field variations at the edges of the rectangular patch, which causes less accurate results.

2.3 Method of Moments

In the analysis of electromagnetic radiation/scattering from microstrip antennas, mostly full-wave numerical methods, such as Method of Moments, Finite Element, Finite Difference Time Domain, are preferred to obtain more accurate results. In this thesis, Method of Moments is chosen to investigate patch antennas, since it can be easily applied to planar antenna structures and solution time is relatively short compared to other mentioned numerical methods.

Method of moments can be applied to solve integral equations of the form

$$\int_{\Omega} k(x,x')f(x')d\Omega = g(x') \tag{2.20}$$

Ω is a geometric domain that can be a curve, surface or volume and $x \in d\ \Omega$.
Equation (2.20) can be written in an operator form as

$$L(f)=g \tag{2.21}$$

where g is a known source distribution, L is a linear operator operating on f and f is the unknown function that will be solved.

Firstly Ω domain is divided into sub domains that satisfy $\Omega = \bigcup_{j=1}^{N} \Omega_j$ or an entire domain solution can be applied that does not require division. Second step is to

choose a set of functions that will be used to approximate unknown function f such that

$$f(x') = \sum_{j=1}^{N} \alpha_j f_j(x') \tag{2.22}$$

$f_j(x')$s are called *basis function*, α_js are unknown coefficients that will be solved. Substituting (2.22) into (2.21)

$$L\left\{\sum_{j=1}^{N} \alpha_j f_j(x')\right\} = g \tag{2.23}$$

Using linearity (2.23) can be written as

$$\sum_{j=1}^{N} \alpha_j L\{f_j(x')\} = g \tag{2.24}$$

Next step is to choose a set of functions to obtain *N* equations with *N* unknowns. This function is called *weighting function,* w_i , and by taking inner product, above equation becomes

$$\sum_{j=1}^{N} \alpha_j \langle L(f_j), w_i \rangle = \langle g, w_i \rangle \tag{2.25}$$

This results in a matrix equation of the form $Ax=b$ where

$$x = \begin{bmatrix} \alpha_1 \\ \alpha_2 \\ . \\ . \\ \alpha_N \end{bmatrix}$$

$$A = \begin{bmatrix} \beta_{11} & \beta_{12} & . & . & \beta_{1N} \\ . & . & . & . & . \\ . & . & . & . & . \\ . & . & . & . & . \\ \beta_{1N} & . & . & . & \beta_{NN} \end{bmatrix} \qquad \beta_{ij} = \left\langle L(f_j), w_i \right\rangle$$

$$b = \begin{bmatrix} \left\langle g, w_1 \right\rangle \\ \left\langle g, w_{21} \right\rangle \\ . \\ . \\ \left\langle g, w_N \right\rangle \end{bmatrix} \tag{2.26}$$

A matrix and b vector is known, unknown x vector can be calculated as

$$x=A^{-1}b \tag{2.27}$$

Inner product of two functions is calculated as

$$\left\langle f_1(x), f_2(x) \right\rangle = \int_{\Omega} f_1(x) f_2^*(x) d\Omega \tag{2.28}$$

$f_2^*(x)$: complex conjugate of $f_2(x)$

Accuracy of the moment method solution depends on the choice of basis and weighting functions. Basis function should be such that equation (2.22) approximates f well. In the analysis of microstrip patch antennas, piecewise sinusoidal basis functions are used in this thesis.

An example of a weighting function is Dirac-Delta function. MoM formulation using Dirac Delta function as weighting is called point matching and can be written as

$$w_i(x') = \delta(x' - x_i) \tag{2.29}$$

where x' is the position vector, x_i is the position of impulse.

In the MoM formulation given in this thesis, Galerkin type weighting functions are used. In this approach, weighting functions are chosen identical to basis functions which are piecewise sinusoidal [12].

Microstrip patch antennas with different feeds are analyzed in this thesis by using MoM. Integral equations that satisfy the boundary conditions of the related structure are obtained by using spectral domain Green's function representations. Then MoM is used to convert these integral equations to a system of linear equations. Matrix equations of the form $Z.I = V$ are solved for current coefficients in vector *I*. Detailed MoM/Green's function formulation of each type of antenna is given in Chapter 3.

CHAPTER 3

MOM FORMULATION OF MICROSTRIP PATCH ANTENNAS USING SPECTRAL DOMAIN GREEN'S FUNCTIONS

MoM/Green's function formulation of a microstrip line, microstrip line fed patch, proximity coupled microstrip patch antenna and slot coupled microstrip patch antenna are given in this chapter. Integral equations for unknown surface currents on line, patch and slots are obtained from boundary conditions of the equivalent problem of related structures using spectral domain representation of Green's functions. Then, MoM is applied to convert integral equation to linear system of equations. Spectral domain Green's function representations used in this thesis are presented for electric and magnetic type sources. It is assumed that dielectric slab and ground plane are infinite in x-y plane. For each microstrip antenna structure details of formulation are given. The evaluation of MoM impedance matrix and voltage vector elements is discussed. Calculation of the input impedance of a microstrip antenna is also presented.

3.1 Spectral Domain Green's Functions for Planar Grounded Dielectric Slabs

In this thesis, MoM formulations for the analysis of microstrip antennas with different feed techniques are obtained. For each structure, Green's functions for the related case are required to evaluate electric and magnetic fields due to currents on line, patch and slot. Green's functions used in the analysis carried out in this thesis are as follows:

G^a_{EJyy} : y directed electric field at (x, y, d_a) due to a y directed infinitesimally small electric current density at (x_0, y_0, d_a) for the geometry shown in Figure 3.1 (a), [7].

G^a_{EMyx} : y directed electric field at (x, y, d_a) due to a x directed infinitesimally small magnetic current density at $(x_0, y_0, 0)$ for the geometry shown in Figure 3.1 (b), [7].

G^a_{HJxy} : x directed magnetic field at $(x, y, 0)$ due to a y directed infinitesimally small electric current density at (x_0, y_0, d_a) for the geometry shown in Figure 3.1 (a), [7].

G^a_{HMxx} : x directed magnetic field at $(x, y, 0)$ due to a x directed infinitesimally small magnetic current density at $(x_0, y_0, 0)$ for the geometry shown in Figure 3.1 (b), [7].

G^a_{EJyy1} : y directed electric field at (x, y, d_{a2}) due to a y directed infinitesimally small electric current density at (x_0, y_0, d_{a2}) for the geometry shown in Figure 3.1 (c), [13].

G^a_{EJyy2} : y directed electric field at (x, y, d_{a1}) due to a y directed infinitesimally small electric current density at (x_0, y_0, d_{a2}) for the geometry shown in Figure 3.1 (c), [13].

G^a_{EJyy3} : y directed electric field at (x, y, d_{a2}) due to a y directed infinitesimally small electric current density at (x_0, y_0, d_{a1}) for the geometry shown in Figure 3.1 (d), [13].

Spectral domain representation of Greens function that represent y directed electric field at (x, y, d_a) due to a infinitesimally small y directed electric current element at (x_0, y_0, d_a) the geometry shown in Figure 3.1 (a) is written as

$$G^a_{EJyy}(x, y, d_a \Big| x_0, y_o, 0) = \int_{-\infty}^{\infty}\int_{-\infty}^{\infty} Q^a_{EJyy}(k_x, k_y) e^{jk_x(x-x_0)} e^{jk_y(y-y_0)} dk_x dk_y \qquad (3.1)$$

All other Greens' functions can be written in the same form, and required kernel functions are:

$$Q^a_{EJyy}(k_x,k_y) = -j\frac{Z_0\sin(k_{1a}d_a)}{4\pi^2 k_0}\frac{(\varepsilon_r^a k_0^2 - k_y^2)k_2\cos(k_{1a}d_a) + j(k_0^2 - k_y^2)k_{1a}\sin(k_{1a}d_a)}{T_e^a T_m^a} \tag{3.2}$$

$$Q^a_{EMyx}(k_x,k_y) = \frac{1}{4\pi^2}\frac{-\varepsilon_r^a k_{1a}k_2\cos(k_{1a}d_a) + j(k_y^2(\varepsilon_r^a - 1) - k_{1a}^2)\sin(k_{1a}d_a)}{T_e^a T_m^a} \tag{3.3}$$

$$Q^a_{HJxy}(k_x,k_y) = -Q^a_{EMyx}(k_x,k_y) \tag{3.4}$$

$$Q^a_{HMxx}(k_x,k_y) = \frac{-j}{4\pi^2 k_0 Z_0}\frac{1}{k_{1a}T_e^a T_m^a}\left[\begin{array}{l} jk_x^2k_{1a}^2(\varepsilon_r^a - 1) + (\varepsilon_r^a k_0^2 - k_x^2) \\ *\left\{\begin{array}{l} k_{1a}k_2(\varepsilon_r^a + 1) \\ *\sin(k_{1a}d_a) \\ \cos(k_{1a}d_a) + j \\ (\varepsilon_r^a k_2^a \sin^2(k_{1a}d_a) \\ -k_{1a}^2\cos^2(k_{1a}d_a)) \end{array}\right. \end{array}\right] \tag{3.5}$$

$$Q^a_{EJyy1}(k_x,k_y) = \frac{-jZ_0}{4\pi^2 k_0}\sin k_{1a}d_{a2} * \left\{\begin{array}{l} \dfrac{(\varepsilon_r^a k_0^2 - k_y^2)(k_{1a}\cos k_{1a}(d_{a1} - d_{a2}) + jk_2\sin k_{1a}(d_{a1} - d_{a2})}{\varepsilon_r^a T_e^a k_{1a}} - \\ \dfrac{j(\varepsilon_r^a - 1)k_y^2 k_{1a}\sin k_{1a}d_{a2}}{\varepsilon_r^a T_e^a T_m^a} \end{array}\right\} \tag{3.6}$$

$$Q^a_{EJyy2}(k_x,k_y) = \frac{-jZ_0}{4\pi^2 k_0}\left\{\frac{(\varepsilon_r^a k_0^2 - k_y^2)T_m^a - jk_y^2 k_{1a}(\varepsilon_r^a - 1)\sin k_{1a}d_{a1}}{\varepsilon_r^a T_e^a T_m^a}\right\}\sin k_{1a}d_{a2} \tag{3.7}$$

$$Q^a_{EJyy3}(k_x,k_y) = Q^a_{EJyy2}(k_x,k_y) \tag{3.8}$$

where

$$
\begin{aligned}
&k_0^2 = w^2 \mu_0 \varepsilon_0 \\
&Z_0 = (\mu_0 / \varepsilon_0)^{1/2} \\
&k_{1a} = \left(\varepsilon_r^a k_0^2 - \beta^2\right)^{1/2} \qquad \mathrm{Im}(k_{1a}) < 0 \qquad \mathrm{Re}(k_{1a}) > 0 \\
&k_2 = \left(k_0^2 - \beta^2\right)^{1/2} \qquad \mathrm{Im}(k_2) < 0 \qquad \mathrm{Re}(k_2) > 0 \\
&T_e^a = k_{1a} \cos(k_{1a} d_a) + j k_2 \sin(k_{1a} d_a) \\
&T_m^a = \varepsilon_r^a k_2 \cos(k_{1a} d_a) + j k_{1a} \sin(k_{1a} d_a)
\end{aligned}
\tag{3.9}
$$

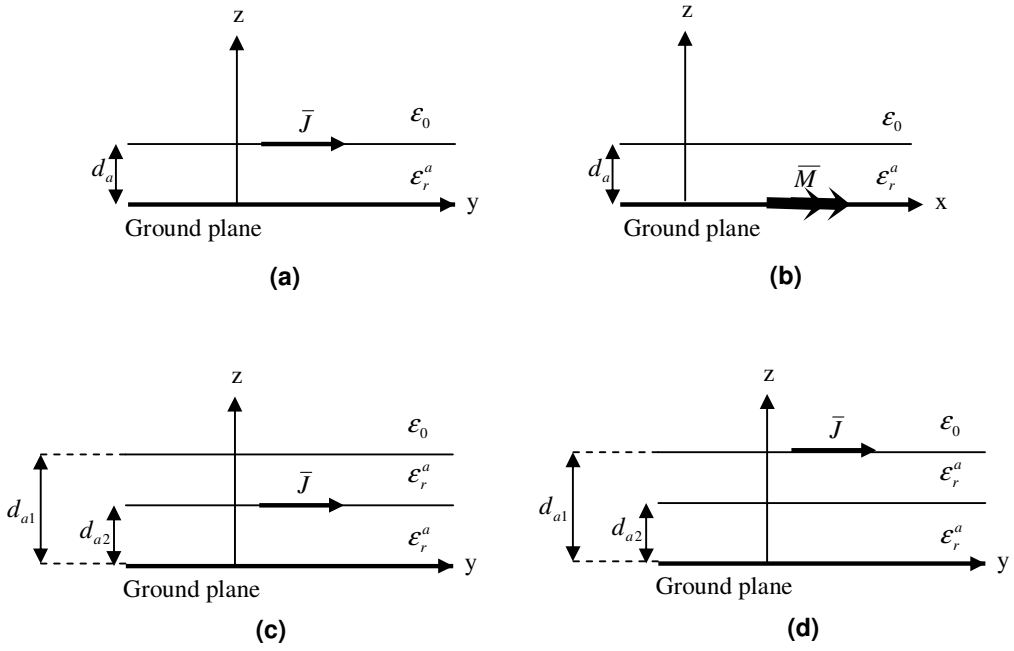

Figure 3.1 - Geometries for spectral domain Green's functions

3.2 MoM Formulation of Microstrip Line

In this part an open circuited microstrip line located on an infinitely large dielectric substrate and ground plane is analyzed, which is shown in Figure 3.2. Current flowing on the line is assumed *y* directed and expanded in terms of piecewise sinusoidal basis functions as

$$\bar{J}_f(x,y) = \sum_{N=1}^{N_a} I_n \bar{J}_n^a(x,y) \tag{3.10}$$

where I_n's are unknown coefficients and basis functions are expressed as

$$\bar{J}_n^a(x,y) = \frac{1}{W_f} \frac{\sin k_e^a \left(h^a - |y - y_n|\right)}{\sin k_e^a h^a} \qquad \begin{array}{l} -W_f/2 \le x \le W_f/2 \\ y_n - h^a \le y \le y_n + h^a \end{array} \tag{3.11}$$

$$h^a = L_f/(N_a + 1)$$

where h^a is the half width of the line basis function, N_a is the number of basis functions taken on the line. It is assumed that x variation of current is uniform. Propagation constant k_e^a of dielectric region *a* is calculated as

$$u = W_f / d_a$$

$$\varepsilon_{re}^a = \frac{\varepsilon_r^a + 1}{2} + \frac{\varepsilon_r^a - 1}{2}\left(1 + \frac{10}{u}\right)^{-cb}$$

$$c = 1 + \frac{1}{49}\ln\left(\frac{u^4 + \left(\frac{u}{52}\right)^2}{u^4 + 0.432}\right) + \frac{1}{18.7}\ln\left[1 + \left(\frac{u}{18.1}\right)^3\right]$$

$$b = 0.564\left(\frac{\varepsilon_r^a - 0.9}{\varepsilon_r^a + 3}\right)^{0.053} \tag{3.12}$$

$$\lambda_a = \lambda_0 / \sqrt{\varepsilon_{re}^a}$$

$$k_e^a = 2\pi / \lambda_a$$

Source current on the feed line is a unit magnitude half PWS basis function located at the beginning of the line. Its expression is given as

$$J_{inc}(x,y) = \frac{1}{W_f}\frac{\sin k_e^a\left(h^a - y\right)}{\sin k_e^a h^a} \qquad \begin{matrix} -W_f/2 \le x \le W_f/2 \\ 0 \le y \le h^a \end{matrix} \tag{3.13}$$

y=0 at the beginning of the line.

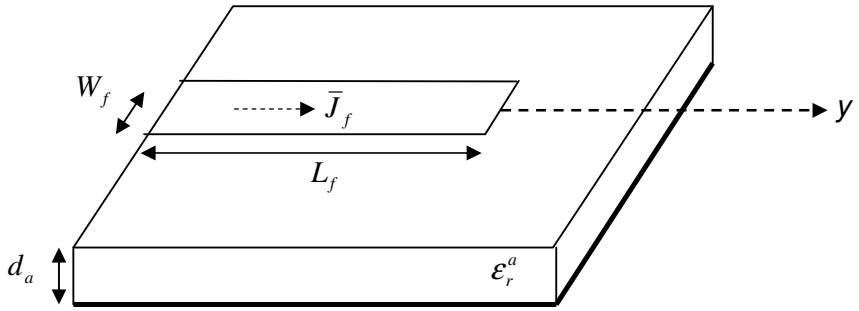

Figure 3.2 – Microstrip line

Representation of line and source basis function on the line is shown in Figure 3.3.

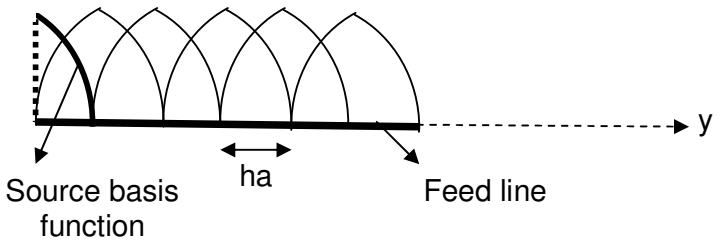

Figure 3.3 – Source and microstrip line basis functions

In order to find unknown current coefficients, an electric field integral equation is obtained from boundary condition stated as tangential component of total electric field should vanish on the line:

$$\overline{E}_a(J_{inc}) + \overline{E}_a(J_f) = 0 \tag{3.14}$$

When calculating electric fields, Green's function given in (3.2) is used. Substituting (3.2) , (3.10) and (3.13) in (3.14), the following expression is obtained:

$$\overline{E}_a(J_{inc}(x_o, y_o)) + \overline{E}_a(\sum_{n=1}^{N_a} I_n^a \overline{J}_n^a(x_o, y_o)) = 0$$

$$\iint_{feed} J_{inc}(x_o, y_o) \int_{-\infty}^{\infty}\int Q_{EJyy}^a(k_x, k_y) e^{jk_x(x-x_o)} e^{jk_y(y-y_o)} + \tag{3.15}$$

$$\iint_{feed} \sum_{n=1}^{N_a} I_n^a \overline{J}_n^a(x_o, y_o) \int_{-\infty}^{\infty}\int Q_{EJyy}^a(k_x, k_y) e^{jk_x(x-x_o)} e^{jk_y(y-y_o)} dk_x dk_y dx_o dy_o = 0$$

After Galerkin weighting is applied, following linear system of equations is obtained.

$$\iint_{feed} J_m^a(x\ ,y\ ) \iint_{feed} J_{inc}(x_o, y_o) \int_{-\infty}^{\infty}\int Q_{EJyy}^a(k_x, k_y) e^{jk_x(x-x_o)} e^{jk_y(y-y_o)} dk_x dk_y dx_o dy_o dxdy +$$

$$\sum_{N=1}^{N_a} I_n^a \iint_{feed} J_m^a(x\ ,y\ ) \iint_{feed} J_n^a(x\ ,y\ ) \int_{-\infty}^{\infty}\int Q_{EJyy}^a(k_x, k_y) e^{jk_x(x-x_o)} e^{jk_y(y-y_o)} dk_x dk_y dx_o dy_o dxdy$$

$$= 0 \tag{3.16}$$

Equation (3.14) can be written in Matrix equation form as follows

$$[V_1] + [Z^a][I^a] = 0 \tag{3.17}$$

$$V_{1m} = -\int_{-\infty-\infty}^{\infty}\int^{\infty} Q_{EJyy}^a(k_x, k_y) \tilde{J}_m^{a*}(k_x, k_y) \tilde{J}_{inc}^a(k_x, k_y) dk_x dk_y \tag{3.18}$$

$$Z_{mn}^a = \int_{-\infty-\infty}^{\infty}\int^{\infty} Q_{EJyy}^a(k_x, k_y) \tilde{J}_m^{a*}(k_x, k_y) \tilde{J}_n^a(k_x, k_y) dk_x dk_y \tag{3.19}$$

where $\tilde{J}_{inc}^{a}$, $\tilde{J}_{n}^{a}$, $\tilde{J}_{m}^{a*}$ are two dimensional Fourier transforms of source and line basis functions and calculated as

$$\tilde{J}_{inc}^{a}(k_x,k_y)=\int_{y_0}\int_{x_0} J_{inc}^{a}(x_0,y_0)e^{-j(k_x x_0+k_y y_0)}dx_0dy_0$$
$$\tilde{J}_{m}^{a*}(k_x,k_y)=\int_{y}\int_{x} J_{m}^{a}(x,y)e^{j(k_x x+k_y y)}dxdy$$
$$\tilde{J}_{n}^{a}(k_x,k_y)=\int_{y_0}\int_{x_0} J_{n}^{a}(x_0,y_0)e^{-j(k_x x_0+k_y y_0)}dx_0dy_0 \qquad (3.20)$$

Matrices in (3.17) have the following dimensions.

V_1 : $N_a \times 1$ known voltage vector

Z^a : $N_a \times N_a$ impedance matrix

I^a : $N_a \times 1$ unknown coefficient vector for line current.

Matrix equation (3.17) is solved for I^a, then line current $\bar{J}_f$ is calculated using (3.10).

Reflection coefficient for the microstrip line of two different width on different substrate thickness are calculated by using the above formulation and given in Chapter 4 in comparison with results available in the literature.

3.3 MoM Formulation of Microstrip Line Fed Patch Antenna

In this section, microstrip line fed patch antenna structure, which is shown in Figure 3.4, is analyzed. It consists of a radiating patch that is fed by a microstrip line placed on a grounded dielectric layer. MoM formulation presented in this chapter is based on the formulation given in [13]. Patch and line currents are assumed *y* directed. Basis function on the line and excitation function is chosen similar to (3.11) and (3.13) respectively; propagation constant of the dielectric region is calculated as (3.12).

Patch current is expanded in terms of basis function where I_n^b's are unknown coefficients

$$\bar{J}_p(x,y) = \sum_{n=1}^{N_b} I_n^b \bar{J}_n^b(x,y)$$

$$\bar{J}_n^b(x,y) = \frac{1}{W_p} \frac{\sin\left(k_e^a (h^b - |y - y_n|)\right)}{\sin\left(k_e^a h^b\right)} \hat{y} \qquad W_p/2 \le x \le W_p/2$$

$$y_n - h^b \le y \le y_n + h^b \qquad (3.21)$$

$$h^b = L_p/(N_b + 1)$$

h^b is the half width of patch basis function, N_b is the number of basis functions taken on the patch. It is assumed that x variation of the patch current is uniform.

To provide the continuity of the current flow from the feed line to the patch, basis functions of the line overlaps the patch surface for a distance S.
To solve the patch and line currents, boundary condition (3.14) is modified to

$$\bar{E}_a(J_{inc}) + \bar{E}_a(J_f) + \bar{E}_a(J_p) = 0 \text{ on line and patch} \qquad (3.22)$$

Matrix equation representation of this boundary condition is

$$\begin{bmatrix} Z & C \\ T & Y \end{bmatrix} \begin{bmatrix} I^a \\ I^b \end{bmatrix} = \begin{bmatrix} V_1 \\ V_2 \end{bmatrix} \qquad (3.23)$$

Elements of matrix Z and vector V_1 are defined in (3.19) and (3.18) respectively. T and C are coupling matrices between line and patch basis functions. They are calculated as,

$$C_{ml}^a = \int_{-\infty}^{\infty}\int_{-\infty}^{\infty} Q_{EJyy}^a(k_x,k_y) \tilde{J}_l^b(k_x,k_y) \tilde{J}_m^{a*}(k_x,k_y) dk_x dk_y \qquad (3.24)$$

where

$$\tilde{J}_l^b(k_x,k_y)=\int_{y_0}\int_{x_0} J_l^b(x_0,y_0)e^{-j(k_x x_0+k_y y_0)}dx_0dy_0 \tag{3.25}$$

Matrix elements of T are easily calculated as

$$T_{kn}^a = C_{ml}^a \quad \text{where } k=l \text{ and } m=n. \tag{3.26}$$

Impedance matrix of the patch is

$$Y_{kl}^a = \int_{-\infty}^{\infty}\int_{-\infty}^{\infty} Q_{EJyy}^a(k_x,k_y)\tilde{J}_l^b(k_x,k_y)\tilde{J}_k^{b*}(k_x,k_y)dk_x dk_y \tag{3.27}$$

where

$$\tilde{J}_k^{b*}(k_x,k_y)=\int_{y}\int_{x} J_k^b(x_0,y_0)e^{j(k_x x+k_y y)}dxdy \tag{3.28}$$

Lastly electric field on the patch generated by the source current is calculated as

$$V_{2k} = -\int_{-\infty}^{\infty}\int_{-\infty}^{\infty} Q_{EJyy}^a(k_x,k_y)\tilde{J}_k^{b*}(k_x,k_y)\tilde{J}_{inc}^a(k_x,k_y)dk_x dk_y \tag{3.29}$$

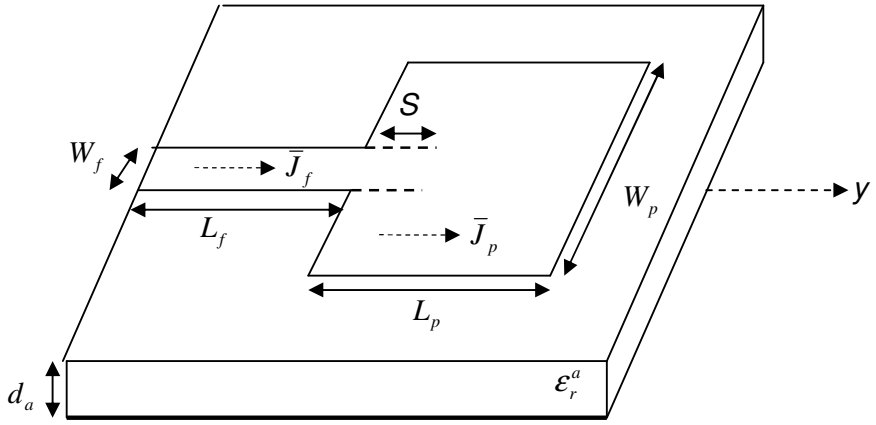

Figure 3.4 – Microstrip line fed patch

Dimensions of matrices and vectors are given as follows

V_1 : $N_a \times 1$ known voltage vector

V_2 : $N_b \times 1$ known voltage vector

Z^a : $N_a \times N_a$ impedance matrix

I^a : $N_a \times 1$ unknown coefficient vector for line

Y^a : $N_b \times N_b$ impedance matrix

I^b : $N_b \times 1$ unknown coefficient vector for patch

C^a : $N_a \times N_b$ matrix

T^a : $N_b \times N_a$ matrix

Matrix equation (3.23) is solved for I^b and I^a, then patch and line currents are calculated using (3.21) and (3.10).

Currents on the line and patch and input impedance of the antenna are calculated for different frequencies by using formulation given in this section and presented in Chapter 4. Furthermore effect of size of overlapping region, length S, is investigated.

3.4 MoM Formulation of Proximity Coupled Microstrip Patch Antenna

A proximity coupled microstrip antenna consists of two dielectric layers separated by a microstrip line. Radiating patch is located at the top of the upper dielectric layer and ground plane is located at the bottom of lower dielectric layer. Figure 3.5 shows the related structure. When microstrip line is excited, fields are coupled to patch from the line. This structure is preferred because of its improved bandwidth. Currents flowing on the patch and line are assumed *y* directed and x variation is uniform. Line and source basis functions are given in (3.11), (3.13) respectively. Propagation constant of patch basis function is different from the one used in Section 3.3. Current density on patch is expanded as

$$\begin{aligned}
&\bar{J}_p(x,y) = \sum_{n=1}^{N_b} I_n^b \bar{J}_n^b(x,y) \\
&\bar{J}_n^b(x,y) = \frac{1}{W_p}\frac{\sin\left(k_e^b(h^b - |y-y_n|\right)}{\sin\left(k_e^b h^b\right)}\hat{y} \qquad x_{0s} - W_p/2 \le x \le x_{0s} + W_p/2 \\
&\qquad\qquad\qquad\qquad\qquad\qquad\qquad\qquad\qquad\qquad y_n - h^b \le y \le y_n + h^b \qquad (3.30) \\
&k_e^b = \sqrt{\varepsilon_{re}^b}\,k_0 \\
&\varepsilon_{re}^b = \left(\varepsilon_r^a + 1\right)/2 + \left(\left(\varepsilon_r^a - 1\right)/2\right)\left(1 + 10d_{a1}/W_p\right)^{-1/2} \\
&h^b = L_p/(N_b + 1)
\end{aligned}$$

In order to solve unknown line and patch current coefficients I^b and I^a, two boundary conditions are written:

1. $\bar{E}^{\tan} = 0$ on the feedline
2. $\bar{E}^{\tan} = 0$ on the patch

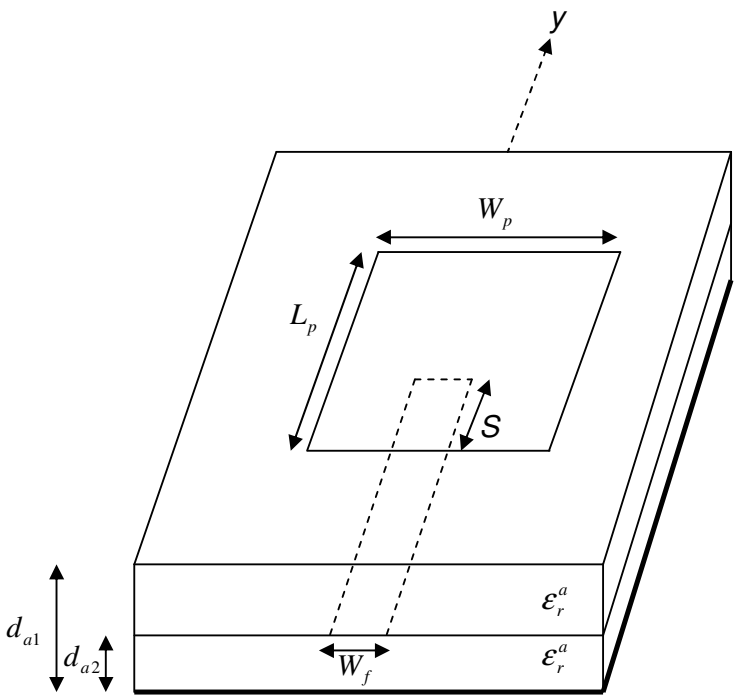

Figure 3.5 – Proximity coupled microstrip antenna

Electric fields can be written in terms of electric currents as:

1. $\overline{E}_a(J_{inc}) + \overline{E}_a(J_f) + \overline{E}_a(J_p) = 0$, on line
2. $\overline{E}_a(J_{inc}) + \overline{E}_a(J_f) + \overline{E}_a(J_p) = 0$, on patch (3.31)

Matrix equation generated for these boundary conditions is same as (3.23) where

$$Z_{mn}^a = \int_{-\infty}^{\infty}\int_{-\infty}^{\infty} Q_{EJyy1}^a(k_x,k_y)\tilde{J}_m^{a*}(k_x,k_y)\tilde{J}_n^a(k_x,k_y)dk_x dk_y \tag{3.32}$$

Green's function of y directed electric field at (x, y, d_{a2}) due to a y directed infinitesimally small electric current density at (x_0, y_0, d_{a2}) is used in the calculation of Z matrix and it is defined in (3.6), [13].

Elements of *C* matrix are calculated as

$$C_{ml}^{a} = \int_{-\infty}^{\infty}\int_{-\infty}^{\infty} Q_{EJyy2}^{a}(k_x,k_y)\tilde{J}_l^{b}(k_x,k_y)\tilde{J}_m^{a*}(k_x,k_y)dk_x dk_y \tag{3.33}$$

Q_{EJyy2}^{a} in this equation is given in (3.7) and it represents *electric field at z=d_{a1} due to infinitesimal y current at z=d_{a2}* while Q_{EJyy}^{a} used in represents *electric field at z=d_a due to infinitesimal y current at z=d_a*

T matrix satisfies (3.26) and it is calculated using *C* matrix.

Formulation of *Y* matrix is similar to (3.21), but basis function and propagation constant is changed to ones given in (3.30)

Patch and line currents, and input impedance are calculated for different frequencies and compared with the results available in the literature and presented in Chapter 4.

3.5 MoM Formulation of Slot Coupled Microstrip Antenna

Figure 3.6 shows the slot coupled microstrip patch antenna structure. Formulation given here is based on the formulation presented in [7]. A slot coupled microstrip antenna is excited from the microstrip line located at the bottom of the structure. A narrow slot is located on the ground plane between the feed line and radiating patch substrates. Fields are coupled to the patch from the microstrip line through the slot on the ground plane.

To analyze this structure, an equivalent problem is defined as shown in Figure 3.7. In the equivalent problem, slot on the ground plane is replaced with *x* directed magnetic currents on above and below the ground plane. In order to satisfy the boundary condition, zero $\overline{E}^{\tan}$ on the ground plane, magnetic current above the ground plane is $\overline{M}_s$ while it is -$\overline{M}_s$ below the ground plane. $\overline{J}_{inc}$ is the only known source current, $\overline{J}_f, \overline{J}_p, \overline{M}_s$ are the unknown currents that will be solved using MoM.

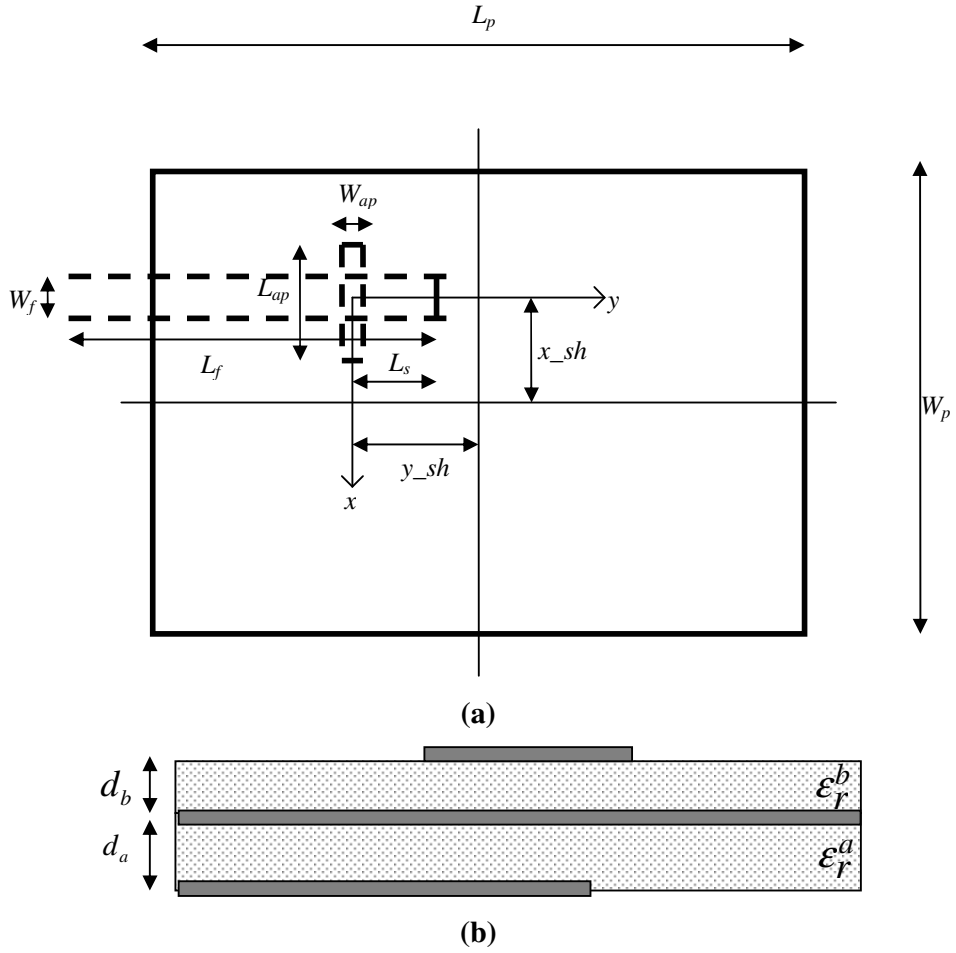

Figure 3.6 – Parameters of aperture coupled microstrip antenna (a) top view (b) side view

In this structure, total electric and magnetic fields in region a (below the ground plane) and region b (above the ground plane) can be written in terms of related currents as:

$$\begin{aligned}
\overline{E}_a^{tot} &= \overline{E}_a\left(\overline{J}_{inc}\right) + \overline{E}_a\left(\overline{J}_f\right) + \overline{E}_a\left(\overline{M}_s\right) \\
\overline{H}_a^{tot} &= \overline{H}_a\left(\overline{J}_{inc}\right) + \overline{H}_a\left(\overline{J}_f\right) + \overline{H}_a\left(\overline{M}_s\right) \\
\overline{E}_b^{tot} &= \overline{E}_b(\overline{J}_p) - \overline{E}_b(\overline{M}_s) \\
\overline{H}_b^{tot} &= \overline{H}_b(\overline{J}_p) - \overline{H}_b(\overline{M}_s)
\end{aligned} \tag{3.34}$$

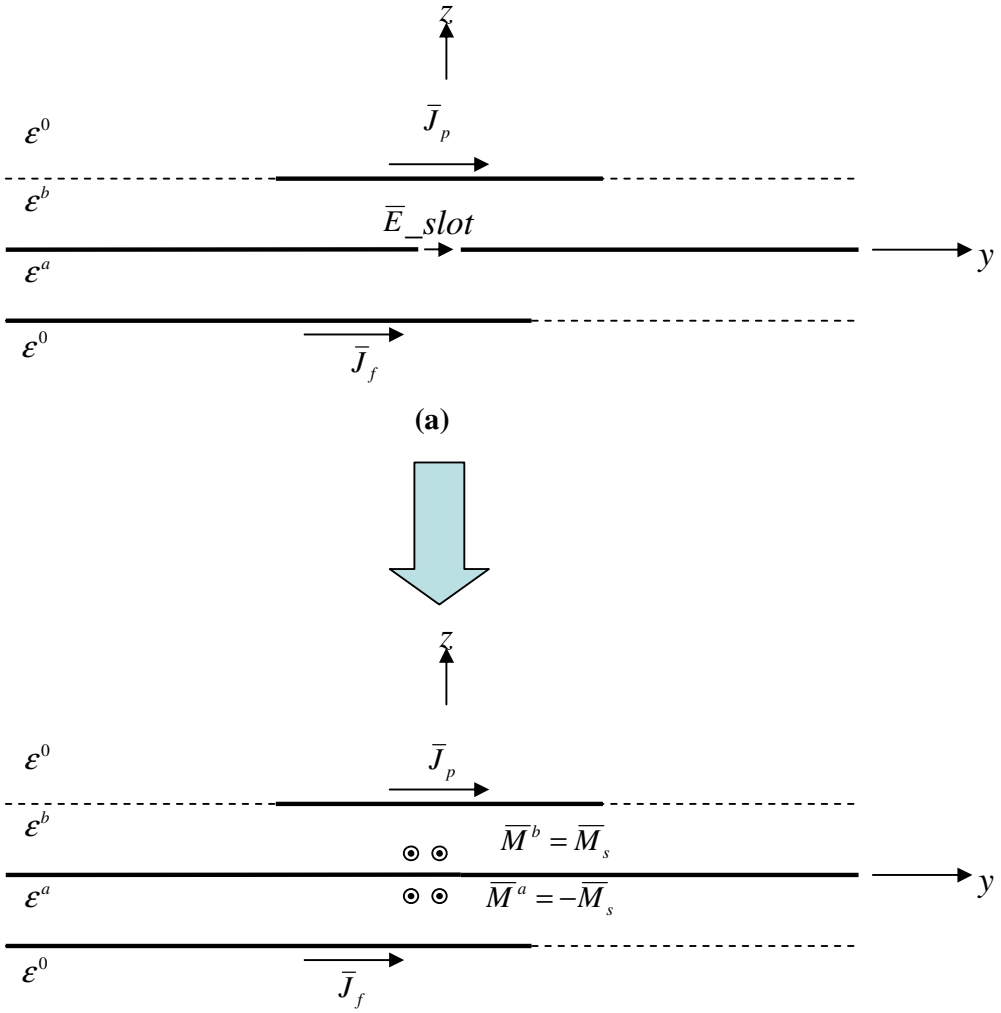

Figure 3.7 – Slot coupled microstrip antenna with (a) surface electric currents (b) with surface electric and magnetic currents

(3.34) means that the total electric and magnetic fields in the region "a" are the sum of electric and magnetic fields generated by the source, line and slot currents. Similarly, total electric and magnetic fields in the region "b" are the sum of electric and magnetic fields generated by patch and slot currents.

Expressions in (3.35) are integral expressions of electric or magnetic fields generated by the patch, slot, incident and feed currents taking into account the dielectric layers and the ground plane:

$$\overline{E}_a(\overline{J}_{inc}) = \iint \hat{y}\hat{y}G^a_{EJyy}(x,y,d_a|x_0,y_0,d_a).\hat{y}\overline{J}_{inc}(x_0,y_0)dx_0dy_0$$

$$\overline{E}_a(\overline{J}_f) = \iint \hat{y}\hat{y}G^a_{EJyy}(x,y,d_a|x_0,y_0,d_a).\hat{y}\overline{J}_f(x_0,y_0)dx_0dy_0$$

$$\overline{E}_a(\overline{M}_s) = \iint \hat{y}\hat{x}G^a_{EMyx}(x,y,d_a|x_0,y_0,0).\hat{x}\overline{M}_s(x_0,y_0)dx_0dy_0$$

$$\overline{H}_a(\overline{J}_{inc}) = \iint_{feed} \hat{x}\hat{y}G^a_{HJxy}(x,y,0|x_0,y_0,d_a).\hat{y}\overline{J}_{inc}(x_0,y_0)dx_0dy_0$$

$$\overline{H}_a(\overline{J}_f) = \iint \hat{x}\hat{y}G^a_{HJxy}(x,y,0|x_0,y_0,d_a).\hat{y}\overline{J}_f(x_0,y_0)dx_0dy_0$$

$$\overline{H}_a(\overline{M}_s) = \iint \hat{x}\hat{x}G^a_{HMxx}(x,y,0|x_0,y_0,0).\hat{x}\overline{M}_s(x_0,y_0)dx_0dy_0$$

$$\overline{E}_b(\overline{J}_p) = \iint \hat{y}\hat{y}G^b_{EJyy}(x,y,d_b|x_0,y_0,d_b).\hat{y}\overline{J}_p(x_0,y_0)dx_0dy_0$$

$$\overline{H}_b(\overline{J}_p) = \iint \hat{x}\hat{y}G^b_{HJxy}(x,y,0|x_0,y_0,d_b).\hat{y}\overline{J}_p(x_0,y_0)dx_0dy_0$$

$$\overline{E}_b(\overline{M}_s) = \iint \hat{y}\hat{x}G^b_{EMyx}(x,y,d_b|x_0,y_0,0).\hat{x}\overline{M}_s(x_0,y_0)dx_0dy_0 \qquad (3.35)$$

$$\overline{H}_b(\overline{M}_s) = \iint \hat{x}\hat{x}G^b_{HMxx}(x,y,0|x_0,y_0,0).\hat{x}\overline{M}_s(x_0,y_0)dx_0dy_0$$

Similar expressions are valid for region b only after replacing ε_r^a to ε_r^b and d_a to d_b. Green's functions are given in (3.2) to (3.7).

In order to find the unknown currents, three integral equations are written using the boundary conditions.

1. $\overline{E}^{\tan} = 0$ on the patch

As given in (3.34) the total electric field in the patch region is the sum of electric field generated by electric patch current and electric field generated by magnetic slot current which can be written on the patch as:

$$\overline{E}_b(\overline{J}_p) + \overline{E}_b(\overline{M}_s) = 0 \qquad (3.36)$$

2. $\overline{E}^{\tan} = 0$ on the feedline

Similarly, equation (3.37) satisfies the second boundary condition.

$$\overline{E}_a(\overline{J}_{inc}) + \overline{E}_a(\overline{J}_f) - \overline{E}_a(\overline{M}_s) = 0 \tag{3.37}$$

3. $\overline{H}^{\tan}$ is continuous through the aperture

$$\overline{H}_b(\overline{J}_p) + \overline{H}_b(\overline{M}_s) = \overline{H}_a(\overline{J}_{inc}) + H_a(\overline{J}_f) - H_a(\overline{M}_s) \tag{3.38}$$

As required in MoM formulations, unknown currents are expanded in terms of known basis functions and unknown coefficients. Basis functions used for the microstrip line and propagation constant of region *a* is given in (3.11) and (3.12). Patch basis function and propagation constant of region *b* is given in (3.30).

Basis function chosen for the magnetic current that represents the aperture is

$$\begin{aligned}
&\overline{M}_s(x,y) = \sum_{N=1}^{N_s} V_n^{\,ap}\, \overline{M}_n^{\,ap}(x,y) \\
&\overline{M}_n^{\,ap}(x,y) = \frac{1}{W_{ap}} \frac{\sin k_{ap}\left(h_{ap} - |x - x_n|\right)}{\sin k_{ap} h_{ap}} \qquad -L_{ap}/2 < x < L_{ap}/2 \\
&\qquad\qquad\qquad\qquad\qquad\qquad -W_{ap}/2 < y < W_{ap}/2 \\
&k_{ap} = \left(k_e^a + k_e^b\right)/2
\end{aligned} \tag{3.39}$$

k_e^a is given in (3.12) and k_e^b is given in (3.30). Incident current on the feed line is a unit magnitude half PWS basis function and expressed as (3.13).

Replacing the unknown currents with PWS basis functions and applying Galerkin type weighting MoM formulation to the integral equations given in (3.36) to (3.38) result in following expressions:

Boundary Condition 1 (3.36):

$$\overline{E}_b(\overline{J}_p) + \overline{E}_b(\overline{M}_s) = 0$$

$$\overline{E}_b\left(\sum_{l=1}^{N_b} I_n^b \overline{J}_n^b(x_o, y_o)\right) - \overline{E}_b\left(\sum_{s=1}^{N_s} V_s^{ap} \overline{M}_s^{ap}(x_o, y_o)\right) = 0$$

$$\iint_{patch} \sum_{l=1}^{N_b} I_l^b \overline{J}_l^b(x_o, y_o) \int_{-\infty}^{\infty}\int Q_{EJyy}^b(k_x, k_y) e^{jk_x(x-x_o)} e^{jk_y(y-y_o)} dk_x dk_y dx_o dy_o - \tag{3.40}$$

$$\iint_{slot} \sum_{s=1}^{N_s} V_s^{ap} \overline{M}_s^{ap}(x_o, y_o) \int_{-\infty}^{\infty}\int Q_{EMyz}^b(k_x, k_y) e^{jk_x(x-x_o)} e^{jk_y(y-y_o)} dk_x dk_y dx_o dy_o = 0$$

V_s^{ap} and I_n^b are coefficients so that they can be taken outside the integration, after weighting above equation is written as

$$\sum_{l=1}^{N_b} I_l^b \iint_{patch} J_k^b(x, y) \iint_{slot} J_l^b(x_o, y_o) \iint Q_{EJyy}^b(k_x, k_y) e^{jk_x(x-x_o)} e^{jk_y(y-y_o)} dk_x dk_y dx_0 dy_o dx dy -$$

$$\sum_{s=1}^{N_s} V_s^{ap} \iint_{patch} J_k^b(x, y) \iint_{slot} M_s^{ap}(x_o, y_o) \iint Q_{EMyx}^b(k_x, k_y) e^{jk_x(x-x_o)} e^{jk_y(y-y_o)} dk_x dk_y dx_0 dy_o dx dy$$

$$= 0 \tag{3.41}$$

This equation results in a matrix equation that can be written as

$$[Z^b][I^b] + [T^b][V^{ap}] = 0 \tag{3.42}$$

where

$$Z_{kl}^b = \int_{-\infty}^{\infty}\int_{-\infty}^{\infty} Q_{EJyy}^b(k_x, k_y) \tilde{J}_k^{b*}(k_x, k_y) \tilde{J}_l^b(k_x, k_y) dk_x dk_y$$

$$T_{ks}^b = \int_{-\infty}^{\infty}\int_{-\infty}^{\infty} Q_{EMyx}^b(k_x, k_y) \tilde{J}_k^{b*}(k_x, k_y) \tilde{M}_s^{ap}(k_x, k_y) dk_x dk_y \tag{3.43}$$

where

$$\tilde{M}_s^{ap}(k_x,k_y)=\int_{y_0}\int_{x_0} M_s^{ap}(x_0,y_0)e^{-j(k_x x_0+k_y y_0)}dx_0dy_0 \tag{3.44}$$

Dimensions of the matrices are as follows:

$Z^b : N_b \times N_b$ matrix

$T^b : N_b \times N_s$ matrix

$I^b : N_b \times 1$ unknown coefficient vector for patch

$V^{ap} : N_b \times 1$ unknown coefficient vector for slot

Boundary Condition 2 (3.37):

$$\begin{aligned}
&\overline{E}_a(\overline{J}_{inc})+\overline{E}_a(\overline{J}_f)-\overline{E}_a(\overline{M}_s)=0\\
&\overline{E}_a(J_{inc}(x_o,y_o))+\overline{E}_a\Big(\sum_{n=1}^{N_a} I_n^a \overline{J}_n^a(x_o,y_o)\Big)-\overline{E}_a\Big(\sum_{N=1}^{N_s} V_n^{ap}\overline{M}_n^{ap}(x_o,y_o)\Big)=0\\
&\iint_{feed} J_{inc}(x_o,y_o)\int_{-\infty}^{\infty}\int Q_{EJyy}^a(k_x,k_y)e^{jk_x(x-x_o)}e^{jk_y(y-y_o)}+\\
&\iint_{feed}\sum_{n=1}^{N_a} I_n^a\overline{J}_n^a(x_o,y_o)\int_{-\infty}^{\infty}\int Q_{EJyy}^a(k_x,k_y)e^{jk_x(x-x_o)}e^{jk_y(y-y_o)}dk_xdk_ydx_ody_o-\\
&\iint_{slot}\sum_{s=1}^{N_s} V_s^{ap}\overline{M}_s^{ap}(x_o,y_o)\int_{-\infty}^{\infty}\int Q_{EMyx}^a(k_x,k_y)e^{jk_x(x-x_o)}e^{jk_y(y-y_o)}dk_xdk_ydx_ody_o=0
\end{aligned} \tag{3.45}$$

After weighting is applied

$$\begin{aligned}
&\iint_{feed} J_m^a(x\ ,y\ )\iint_{feed} J_{inc}(x_o,y_o)\int_{-\infty}^{\infty}\int Q_{EJyy}^a(k_x,k_y)e^{jk_x(x-x_o)}e^{jk_y(y-y_o)}dk_xdk_ydx_ody_odxdy+\\
&\sum_{N=1}^{N_a} I_n^a\iint_{feed} J_m^a(x\ ,y\ )\iint_{feed} J_n^a(x\ ,y\ )\int_{-\infty}^{\infty}\int Q_{EJyy}^a(k_x,k_y)e^{jk_x(x-x_o)}e^{jk_y(y-y_o)}dk_xdk_ydx_ody_odxdy-\\
&\sum_{N=1}^{N_a} V_s^{ap}\iint_{feed} J_m^a(x\ ,y\ )\iint_{slot}\overline{M}_s^{ap}(x_o,y_o)\int_{-\infty}^{\infty}\int Q_{EMyx}^a(k_x,k_y)e^{jk_x(x-x_o)}e^{jk_y(y-y_o)}dk_xdk_ydx_ody_o\\
&dxdy=0
\end{aligned} \tag{3.46}$$

Matrix equation representation is

$$[V_1]+[Z^a][I^a]-[T^a][V^{ap}]=0 \tag{3.47}$$

$$V_{1m} = \int_{-\infty}^{\infty}\int_{-\infty}^{\infty} Q^a_{EJyy}(k_x,k_y)\tilde{J}^{a*}_m(k_x,k_y)\tilde{J}^a_{inc}(k_x,k_y)dk_x dk_y$$

$$Z^a_{mn} = \int_{-\infty}^{\infty}\int_{-\infty}^{\infty} Q^a_{EJyy}(k_x,k_y)\tilde{J}^{a*}_m(k_x,k_y)\tilde{J}^a_n(k_x,k_y)dk_x dk_y \tag{3.48}$$

$$T^a_{mn} = \int_{-\infty}^{\infty}\int_{-\infty}^{\infty} Q^a_{EMyx}(k_x,k_y)\tilde{J}^{a*}_m(k_x,k_y)\tilde{M}_{ap}(k_x,k_y)dk_x dk_y$$

Dimensions of the matrices are as follows:

$V_1 \rightarrow N_a \times 1$ known voltage vector

$Z^a \rightarrow N_a \times N_a$ matrix

$T^a \rightarrow N_a \times N_s$ matrix

$I^a \rightarrow N_a \times 1$ unknown coefficient vector for line

$V^{ap} \rightarrow N_a \times 1$ unknown coefficient vector for slot

Boundary Condition 3 (3.38):

$$\overline{H}_b(\overline{J}_p)+\overline{H}_b(\overline{M}_s)=\overline{H}_a(\overline{J}_{inc})+H_a(\overline{J}_f)-H_a(\overline{M}_s)$$

Boundary condition in terms of basis functions is

$$\overline{H}_b(\sum_{l=1}^{N_b} I_l^b \overline{J}_l^b(x_o, y_o)) + \overline{H}_b(\sum_{s=1}^{N_s} V_s^{ap} \overline{M}_s^{ap}(x_o, y_o) =$$

$$\overline{H}_a(J_{inc}(x_o, y_o)) + \overline{H}_a(\sum_{n=1}^{N_a} I_n^a \overline{J}_n^a(x_o, y_o)) - \overline{H}_a(\sum_{s=1}^{N_s} V_s^{ap} \overline{M}_s^{ap}(x_o, y_o)$$

$$\iint_{patch} \sum_{l=1}^{N_b} I_l^b \overline{J}_l^b(x_o, y_o) \int_{-\infty}^{\infty}\int Q_{HExy}^b(k_x, k_y) e^{jk_x(x-x_o)} e^{jk_y(y-y_o)} dk_x dk_y dx_o dy_o +$$

$$\iint_{slot} \sum_{s=1}^{N_s} V_s^{ap} \overline{M}_s^{ap}(x_o, y_o) \int_{-\infty}^{\infty}\int Q_{HMxx}^b(k_x, k_y) e^{jk_x(x-x_o)} e^{jk_y(y-y_o)} dk_x dk_y dx_o dy_o =$$

$$\iint_{feed} J_{inc}(x_o, y_o) \int_{-\infty}^{\infty}\int Q_{HJxy}^a(k_x, k_y) e^{jk_x(x-x_o)} e^{jk_y(y-y_o)} +$$

$$\iint_{feed} \sum_{n=1}^{N_a} I_n^a \overline{J}_n^a(x_o, y_o) \int_{-\infty}^{\infty}\int Q_{HJxy}^a(k_x, k_y) e^{jk_x(x-x_o)} e^{jk_y(y-y_o)} dk_x dk_y dx_o dy_o -$$

$$\iint_{slot} \sum_{s=1}^{N_{st}} V_s^{ap} \overline{M}_s^{ap}(x_o, y_o) \int_{-\infty}^{\infty}\int Q_{HMxz}^a(k_x, k_y) e^{jk_x(x-x_o)} e^{jk_y(y-y_o)} dk_x dk_y dx_o dy_o \qquad (3.49)$$

After weighting, boundary condition becomes

$$\sum_{n=1}^{N_b} I_n^b \iint_{slot} \overline{M}_r^{ap}(x\ ,y\ ) \iint_{patch} J_n^b(x_o, y_o) \iint Q_{EJyy}^b(k_x, k_y) e^{jk_x(x-x_o)} e^{jk_y(y-y_o)} dk_x dk_y dx_0 dy_o dxdy +$$

$$\sum_{s=1}^{N_s} V_n^{ap} \iint_{slot} \overline{M}_r^{ap}(x\ ,y\ ) \iint_{slot} M_s^{ap}(x_o, y_o) \iint Q_{EMyx}^b(k_x, k_y) e^{jk_x(x-x_o)} e^{jk_y(y-y_o)} dk_x dk_y dx_0 dy_o dxdy$$

$$= \iint_{slot} \overline{M}_r^{ap}(x\ ,y\ ) \iint_{feed} J_{inc}(x_o, y_o) \int_{-\infty}^{\infty}\int Q_{HJxy}^a(k_x, k_y) e^{jk_x(x-x_o)} e^{jk_y(y-y_o)} dk_x dk_y dx_o dy_o dxdy +$$

$$\sum_{N=1}^{N_a} I_n^a \iint_{slot} \overline{M}_r^{ap}(x\ ,y\ ) \iint_{feed} J_n^a(x\ ,y\ ) \int_{-\infty}^{\infty}\int Q_{HJxy}^a(k_x, k_y) e^{jk_x(x-x_o)} e^{jk_y(y-y_o)} dk_x dk_y dx_o dy_o dxdy -$$

$$\sum_{N=1}^{N_s} V_s^{ap} \iint_{slot} \overline{M}_r^{ap}(x\ ,y\ ) \iint_{slot} \overline{M}_s^{ap}(x_o, y_o) \int_{-\infty}^{\infty}\int Q_{HMxx}^a(k_x, k_y) e^{jk_x(x-x_o)} e^{jk_y(y-y_o)} dk_x dk_y dx_o dy_o$$

$$dxdy = \quad 0 \qquad (3.50)$$

Matrix equation for this boundary condition is

$$[C^b][I^b] + [Y^b][V^{ap}] = [C^a][I^a] + [V_2] - [Y^a][V^{ap}] \qquad (3.51)$$

where

$$V_2 = \int_{-\infty}^{\infty}\int_{-\infty}^{\infty} Q^a_{HJxy}(k_x,k_y)\tilde{M}^*_{ap}(k_x,k_y)\tilde{J}^a_{inc}(k_x,k_y)dk_x dk_y$$

$$C^a = \int_{-\infty}^{\infty}\int_{-\infty}^{\infty} Q^a_{HJxy}(k_x,k_y)\tilde{M}^*_{ap}(k_x,k_y)\tilde{J}^a_{n}(k_x,k_y)dk_x dk_y$$

$$Y^a = \int_{-\infty}^{\infty}\int_{-\infty}^{\infty} Q^a_{HMxx}(k_x,k_y)\tilde{M}^*_{ap}(k_x,k_y)\tilde{M}_{ap}(k_x,k_y)dk_x dk_y \qquad (3.52)$$

$$Y^b = \int_{-\infty}^{\infty}\int_{-\infty}^{\infty} Q^b_{HMxx}(k_x,k_y)\tilde{M}^*_{ap}(k_x,k_y)\tilde{M}_{ap}(k_x,k_y)dk_x dk_y$$

$$C^b = \int_{-\infty}^{\infty}\int_{-\infty}^{\infty} Q^b_{HJxy}(k_x,k_y)\tilde{M}^*_{ap}(k_x,k_y)\tilde{J}^b_{l}(k_x,k_y)dk_x dk_y$$

where

$$\tilde{M}^*_{ap}(k_x,k_y) = \int_y\int_x M^{ap}(x,y)e^{j(k_x x + k_y y)}dxdy \qquad (3.53)$$

Dimensions of the matrices are as follows:

$V_2 \rightarrow N_s \times 1$ known voltage vector

$C^a \rightarrow N_s \times N_a$ matrix

$C^b \rightarrow N_s \times N_b$ matrix

$Y^a \rightarrow N_s \times N_s$ matrix

$Y^b \rightarrow N_s \times N_s$ matrix

$I^a \rightarrow N_a \times 1$ unknown coefficient vector for line

$I^b \rightarrow N_b \times 1$ unknown coefficient vector for patch

$V^{ap} \rightarrow N_a \times 1$ unknown coefficient vector for slot

Using (3.42), $[I^b]$ is written in terms of $[V^{ap}]$ using the first boundary condition.

$$\begin{aligned}&[Z^b][I^b]+[T^b]V^{ap}=0\\&\Rightarrow[I^b]=-[Z^b]^{-1}[T^b][V^{ap}]\end{aligned}\tag{3.54}$$

Similarly, it is written for I^a from the second boundary condition as

$$\begin{aligned}&[Z^a][I^a]-[T^a][V^{ap}]=[V_1]\\&\Rightarrow[I^a]=[Z^a]^{-1}([V_1]+[T^a][V^{ap}])\end{aligned}\tag{3.55}$$

Lastly, V_{ap} is found using the third boundary condition.

$$\begin{aligned}&[C^b][I^b]+[Y^b][V^{ap}]+[Y^a][V^{ap}]-[C^a][I^a]=[V_2]\\&\Rightarrow[V^{ap}]=\frac{[V_2]+[C^a][I^a]-[C^b][I^b]}{(Y^a+Y^b)}\\&[V^{ap}]=\frac{[V_2]-[C^a][Z^a]^{-1}[V_1]}{((Y^a+Y^b)-[C^a][Z^a]^{-1}[T^a]-[C^b][Z^b]^{-1}[T^b])}\end{aligned}\tag{3.56}$$

Once $[V^{ap}]$ is found, coefficients for patch and slot, $[I^b]$ and $[I^a]$ respectively, can be found from equations (3.54) and (3.55).

3.6 Evaluation of Integrals in MoM Matrix and Vector Entries

Integrals in all matrix and vector entries given in Section 3.2 to 3.5 are in the form of:

$$\int_{-\infty}^{\infty}\int_{-\infty}^{\infty}(.)dkxdky\tag{3.57}$$

To simplify this integration, following transformation is used.

$$\begin{aligned} kx &= \beta\cos\alpha \\ ky &= \beta\sin\alpha \end{aligned} \tag{3.58}$$

Then, the integration in (3.57) becomes

$$\int_0^{\infty}\int_0^{2\pi}(.)\beta d\alpha d\beta \tag{3.59}$$

Also when calculating $Z_{kl}^{b}, Z_{mn}^{a}, Y_{rs}^{a}, Y_{rs}^{b}$ square matrices generated for all feeding methods, even odd properties of the integrands are used, so that boundaries of α integration is changed from 0: 2π to 0: $\pi/2$, [14]. Then, integral equations can be written in the following expressions

$$\begin{aligned} Z_{kl}^{b} &= 4\int_0^{\infty}\int_0^{\pi/2} Q_{EJyy}^{b}(k_x,k_y)\,\mathrm{Re}\{\ \tilde{J}_k^{b*}(k_x,k_y)\tilde{J}_l^{b}(k_x,k_y)\ \}\beta d\alpha\ d\beta \\ Z_{mn}^{a} &= 4\int_0^{\infty}\int_0^{\pi/2} Q_{EJyy}^{a}(k_x,k_y)\,\mathrm{Re}\{\ \tilde{J}_m^{a*}(k_x,k_y)\tilde{J}_n^{a}(k_x,k_y)\ \}\beta d\alpha\ d\beta \\ Y_{rs}^{a} &= 4\int_0^{\infty}\int_0^{\pi/2} Q_{HMxx}^{a}(k_x,k_y)\,\mathrm{Re}\{\ M_r^{ap*}(k_x,k_y)M_s^{ap}(k_x,k_y)\ \}\beta d\alpha\ d\beta \\ Y_{rs}^{b} &= 4\int_0^{\infty}\int_0^{\pi/2} Q_{HMxx}^{b}(k_x,k_y)\,\mathrm{Re}\{\ M_r^{ap*}(k_x,k_y)M_s^{ap}(k_x,k_y)\ \}\beta d\alpha\ d\beta \end{aligned} \tag{3.60}$$

In the numerical calculation, upper limit of β integral is determined based on experience. For each matrix element generated during solution, convergence of terms is tested. Real part of these terms converges near k_0 while the imaginary part needs a larger upper limit. Experiments on all the matrix elements have shown that $200k_0$ is sufficient for the upper limit. When the upper limit is changed to $400k_0$, no significant change is observed in the values of matrix elements.

Both α and β integrations are handled using Gaussian quadrature technique. α integration from 0 to π/2 in (3.60) is divided into 7 pieces and α integration from 0 to 2π is divided into 31 pieces for the rest of the matrices which means α integration is handled in π/16 intervals. For each interval Gaussian quadrature of order 16 is used in both cases. β integration from 0 to $200k_0$ is handled in 200 pieces. Gaussian quadrature of order 16 is used for each piece. Different intervals and orders of Gaussian quadrature cases are tried during the study and parameters given above provided the most accurate results.

3.7 Singularity Treatment

There is always at least one TM surface wave pole that needs a special treatment. This pole occurs at a real β value for a lossless medium and its location is in the range $k_0 \le \beta_p < \sqrt{\varepsilon_r} k_0$. To prevent a numerical difficulty when integrating for $\beta = \beta_p$ integrals are modified as

$$\int_0^\infty f(\beta)d\beta = \int_0^\infty \left(f(\beta) - \frac{\mathrm{Re}\, s}{\beta - \beta_p} \right) d\beta + \int_0^\infty \frac{\mathrm{Re}\, s}{\beta - \beta_p} d\beta \tag{3.61}$$

where

$$\begin{aligned} \int_0^\infty \frac{\mathrm{Re}\, s}{\beta - \beta_p} d\beta &= \int_0^{\beta_p - \varepsilon} \frac{\mathrm{Re}\, s}{\beta - \beta_p} d\beta + \int_{\beta_p - \varepsilon}^{\beta_p + \varepsilon} \frac{\mathrm{Re}\, s}{\beta - \beta_p} d\beta + \int_{\beta_p + \varepsilon}^\infty \frac{\mathrm{Re}\, s}{\beta - \beta_p} d\beta \\ &= -\pi j \,\mathrm{Re}\, s + \mathrm{Re}\, s * \ln\left(\frac{400k_0 - \beta_p}{\beta_p} \right) \end{aligned} \tag{3.62}$$

Res in (3.62) represents the residue of the integrand at the pole.

3.8 Calculation of Reflection Coefficient and Input Impedance

To find the reflection coefficient for different cases formulated through section 3.2 to 3.5, a method called Prony's Exponential Fitting Method [15], is used. This method approximates the feed current as a summation of two waves one of which moves in +y direction while the other moves in –y direction. It is written according to the position on the line as

$$I(y) = C^{+} e^{-\gamma_1 y} + C^{-} e^{\gamma_2 y} \tag{3.63}$$

where γ_1 and γ_2 are the wave numbers for the waves moving in +y and –y directions respectively. It is expected that $\gamma_1 = \gamma_2$. Although in the numerical solution these numbers are not exactly identical to each other but for a good fitting they are close enough to each other. γ_1 and γ_2 are also close to the propagation constant k_e^a given in (3.12). C^{+} and C^{-} are the coefficients of the waves. Current reflection coefficient at the beginning of the microstrip line, after this exponential fitting is applied, is found as

$$\Gamma = \frac{C^{-}}{C^{+}} \tag{3.64}$$

Phase reference of input impedance for microstrip line fed patch antenna is the radiating edge of the patch where line is connected; for the proximity coupled patch, input impedance is referenced at the open end of microstrip feed line. In the slot coupled microstrip antenna problem, input impedance is referenced to the center of the aperture. Input impedance is calculated for all cases as

$$Z_{in} = \frac{1 - \Gamma\, e^{j2k_e^a L_f}}{1 + \Gamma\, e^{j2k_e^a L_f}} \tag{3.65}$$

where L_f is the distance from the beginning of line to reference plane.

CHAPTER 4

NUMERICAL RESULTS

4.1 Introduction

In this chapter numerical results obtained for microstrip patch antennas with different feeding techniques are given, compared with the results available in literature and discussed. Computer code based on Method of Moment formulation given in chapter 3, has been developed and used to obtain numerical results.

4.2 Evaluation of the Self Impedance and Mutual Impedance Between Two Current Elements

As known from equation (3.42), Z_{kl}^{b} represents the impedance matrix of a rectangular patch located on a grounded dielectric substrate. Firstly, results calculated for Z_{kl}^{b} matrix by the developed Fortran code are checked.

To obtain Z_{kl}^{b}, a rectangular patch with width, W_patch, of 0.3λ, and length, L_patch, of 0.3 λ is chosen for the frequency 300MHz. Thickness of the dielectric is chosen as 0.04λ and the dielectric constant of the substrate is 2.55. Number of basis functions used for the patch is 3, so that Z_{kl}^{b} is a 3x3 matrix. Table 4.1 shows the elements of Z_{kl}^{b} matrix.

Table 4.1 – Elements of 3x3 Z_{kl}^{b} matrix

Z_{kl}^{b}	l=1	L=2	l=3
k=1	-0.43675 + 27.66i	-0.41976 - 18.524i	-0.37119 - 5.5783i
k=2	-0.41976 - 18.524i	-0.43675 + 27.66i	-0.41976 - 18.524i
k=3	-0.37119 - 5.5783i	-0.41976 - 18.524i	-0.43675 + 27.66i

As expected, Z_{kl}^{b} is a Toeplitz matrix, so that it is sufficient to evaluate the first row of the impedance matrix.

$$Z_{11}^{b} = Z_{22}^{b} = Z_{33}^{b}$$
$$Z_{12}^{b} = Z_{21}^{b} = Z_{23}^{b} = Z_{32}^{b}$$
$$Z_{13}^{b} = Z_{31}^{b}$$

When calculating impedance matrix elements, infinite integration on β is taken in the range 0 to $200k_0$. To be sure that integrals of matrix elements are converged, the upper limit is changed to $400k_0$. When the integral limit is changed, real part of the matrix elements remained constant. Only a small difference occurred in the imaginary part. To save from computation time, it is decided to terminate the integration at $200k_0$.

To check the convergence of integrals in Z_{kl}^{b} matrix imaginary part of self impedance term is plotted in Figure 4.1., and Re(Z_{11}^{b}) is constant at 0.43675. Similarly, convergence graph for mutual impedance is given in Figure 4.2., and Re(Z_{12}^{b}) is constant at 0.41976.

Next, basic rectangular patch structure is modified to 2 patches with 0.5λ separation. Each patch has W_patch and L_patch of 0.3λ. Dielectric constant and substrate thickness are not changed. When 3 basis functions are taken for each patch, total Z_{kl}^{b} matrix is 6x6. New elements of Z matrix are shown in Table 4.2

Table 4.2 – Elements of 6x6 Z Matrix

Zkl	l=1	l=2	l=3	l=4	l=5	l=6
k=1	0.4367 - 27.66i	0.4198 + 18.524i	0.3712 + 5.5783i	-0.0076 - 0.0984i	-0.0563 - 0.0717i	-0.0798 - 0.0304i
k=2	0.4198 + 18.524i	0.4367 - 27.66i	0.4197 + 18.524i	0.0632 - 0.0919i	-0.0077 - 0.0984i	-0.0563 - 0.0717i
k=3	0.3712 + 5.5783i	0.4197 + 18.524i	0.4367 - 27.66i	0.1493 - 0.0202i	0.0632 - 0.0919i	-0.0076 - 0.0984i
k=4	-0.0076 - 0.0984i	0.0632 - 0.0919i	0.1493- 0.0202i	0.4367 - 27.66i	0.4198 + 18.524i	0.3712 + 5.5783i
k=5	-0.0563 - 0.0717i	-0.0077 - 0.0984i	0.0632 - 0.0919i	0.4198 + 18.524i	0.4367 - 27.66i	0.4197 + 18.524i
k=6	-0.0798 - 0.0304i	-0.0563 - 0.0717i	-0.0076 - 0.0984i	0.3712 + 5.5783i	0.4197 + 18.524i	0.4367 - 27.66i

This analysis is carried out to validate the accuracy of the results calculated for the patch region. When matrix elements are compared to the ones obtained for the same cases in [16], it is observed that they are in good agreement.

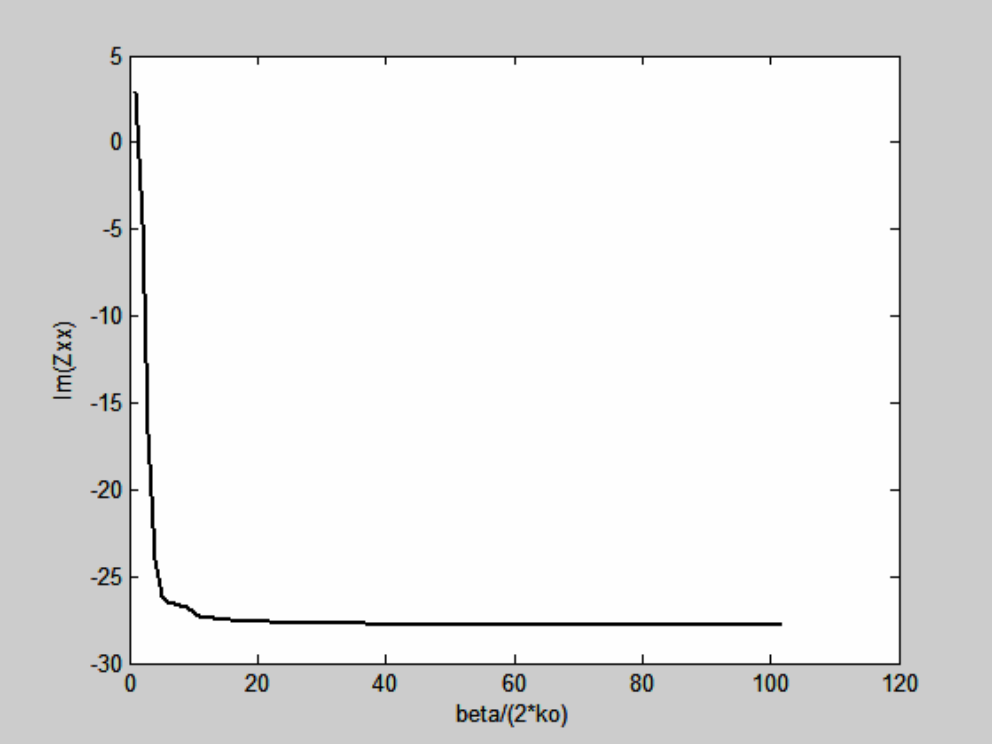

Figure 4.1 – Convergence of imaginary part of self impedance term

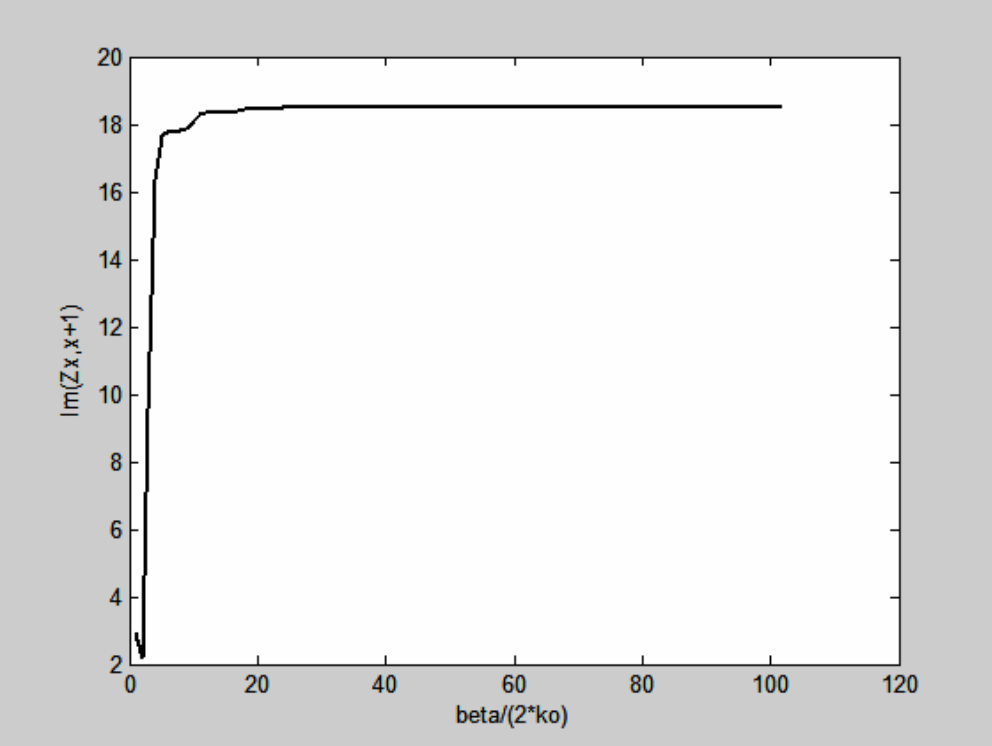

Figure 4.2 – Convergence of imaginary part of mutual impedance term

4.3 Microstrip Feed Line

Analysis of microstrip line, shown in Figure 3.2, is carried out according to the formulation given in section 3.2. Reflection coefficients of the line for different line widths and substrate thicknesses are calculated and presented.

Figure 4.3 shows the variation of the magnitude of reflection coefficient of the line as a function the thickness of the substrate for ε_r of 2.55. Reflection coefficient for a line of width W_f of 0.02λ and W_f of 0.1λ are plotted. These results are compared with the results given in Pozar's paper [17]. In [17], line is assumed to extended to infinity in one direction. Results obtained by the code developed in this thesis show good agreement with results given in [17].

As the thickness of the substrate increases, reflection coefficient of the line gets smaller. It is also seen from the Figure 4.3 that there is an inverse relationship between the width of the line and the value of reflection coefficient.

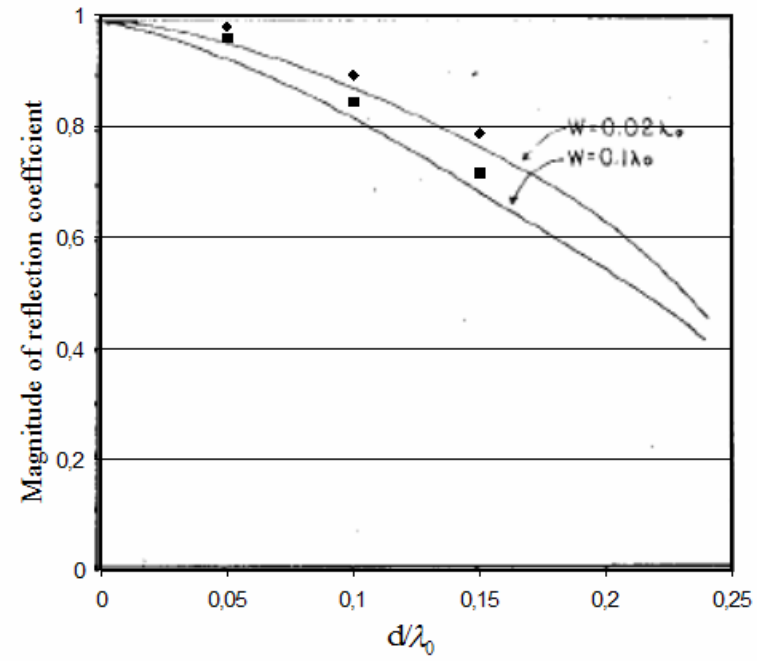

Figure 4.3 – Reflection coefficient versus substrate thickness compared with reflection coefficient given in [17], solid line:[17], markers:calculated

4.4 Microstrip Line Fed Patch

Formulation given in section 3.3 is applied to solve the line and patch currents of a microstrip line fed patch. Furthermore, reflection coefficient and input impedance is calculated for different frequencies.

The width and the length of the patch, W_p and L_p respectively, are 4.02cm. S is chosen 0.45x L_p and 0.65xL_p and results are obtained for both S values. Line width W_f is 0.477cm. Dielectric constant of the substrate is 2.57 and thickness is 0.159cm.

Feed point is always centered at the edge of the patch. Line length is taken 0.15m+S in all cases. Number of basis functions taken on line is 25 while it is 5 for the patch.

Figure 4.4 shows the line current at 2200MHz and 2300MHz. Figure 4.5 gives the patch currents at 2200MHz and 2300MHz. Both of the figures are obtained for the case S/L_p =0.65.

Reflection coefficient and input impedance values at different frequencies are calculated and input impedance results are compared with the ones given in [13]. Smith chart plot of input impedance results obtained by the formulation given in this thesis, -denoted as "calculated" in the Figure 4.6, measured results taken from [13] and calculated by Pozar, [13] are given in Figure 4.6. Results show that impedance value is not extremely dependent on the value of S. Calculated results are in good agreement with measured data and the calculated results in [13]. Note that in [13], line is assumed to extended to infinity in one direction.

4.5 Proximity Coupled Microstrip Antenna

MoM formulation of the proximity coupled microstrip patch antenna is presented in Section 3.4. In this section, currents and input impedance obtained using related formulation are given and compared with the results given in [13].

Analyzed structure has a patch length L_p of 2.5cm. Patch width W_p is 4cm and S/L_p is 0.52. Strip line width W_f is chosen as 0.5cm and line length is 0.1m+S. Permittivity and thickness of both dielectric layers is 2.22 while thicknesses $d_{a1}= 2d_{a2}$ =0.318cm. 25 basis functions are used on line and 5 basis functions are used on patch. Magnitudes of the line and the patch currents at two different frequencies are shown in Figure 4.7 and 4.8. Input impedance calculated by the developed code and Pozar [13] are plotted on a Smith chart and presented in Figure 4.9. The agreement between the results are acceptable.

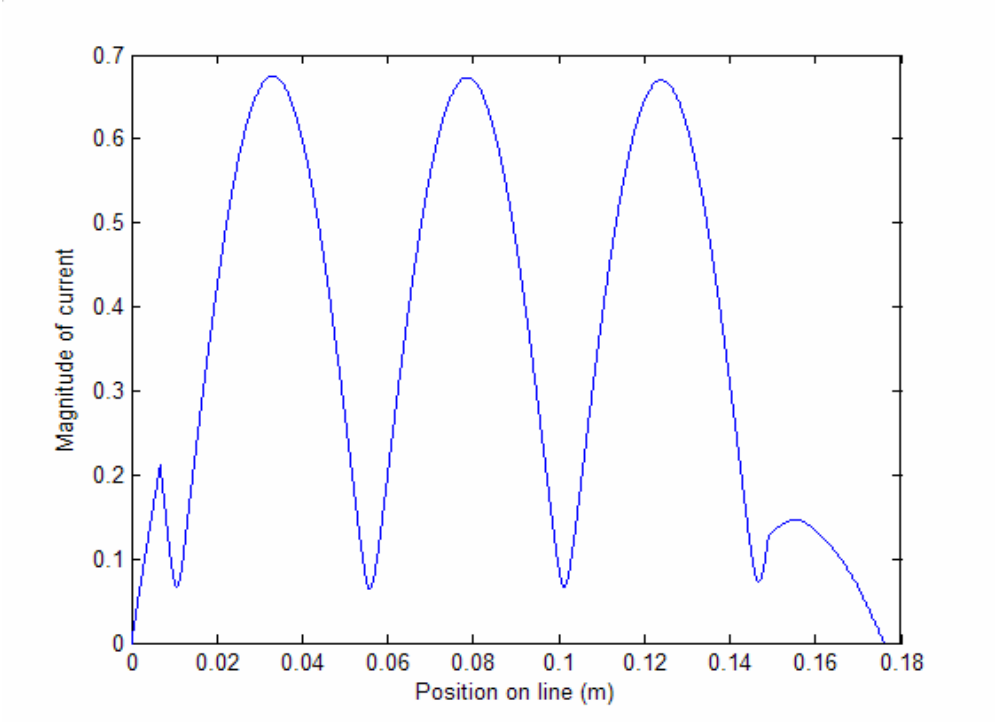

(a)

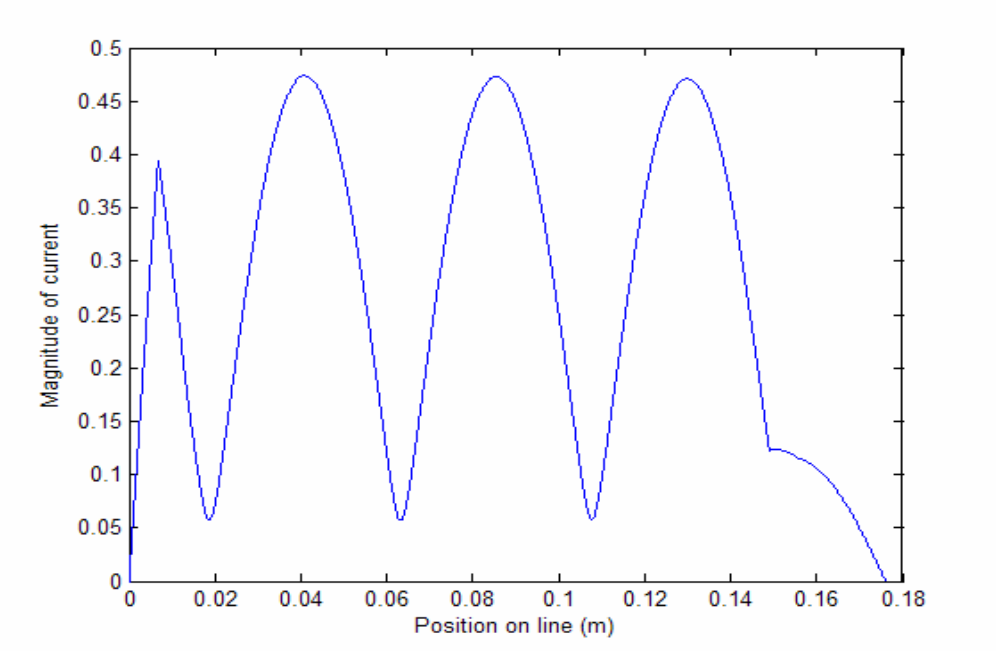

(b)

Figure 4.4 – Magnitude of stripline current at (a) 2200MHz and (b)2300MHz for S/L_p =0.65 in both cases

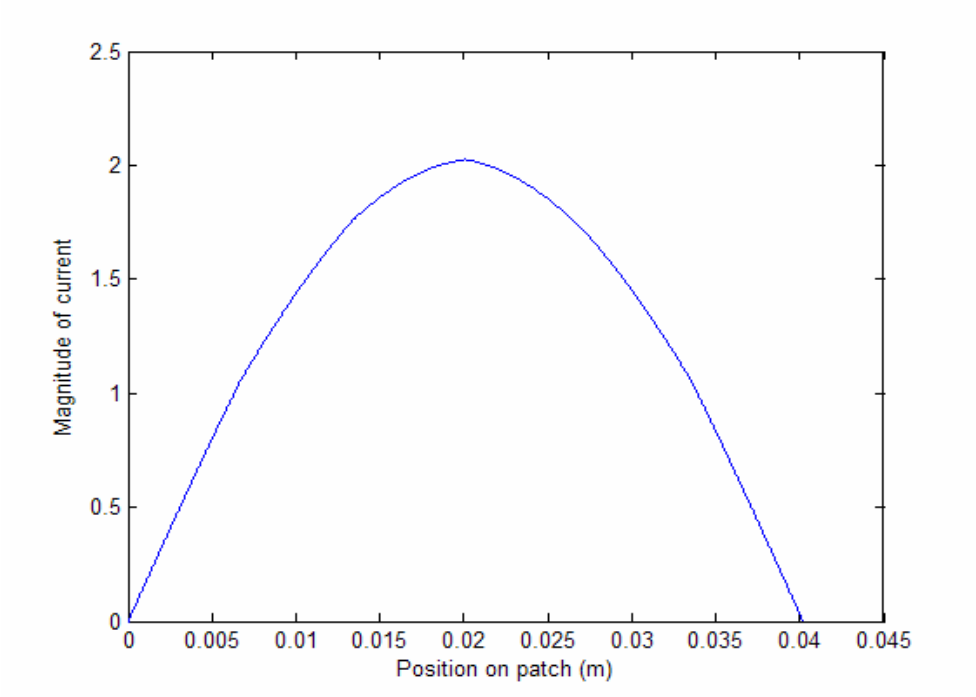

(a)

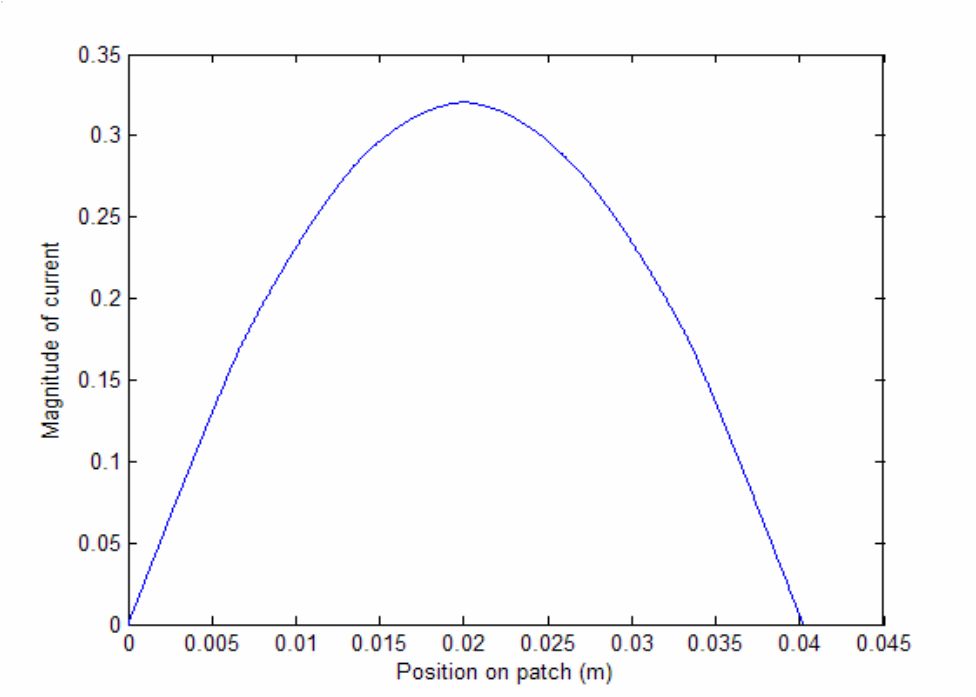

(b)

Figure 4.5 – Magnitude of patch current at (a) 2200MHz and (b)2300MHz for S/L_p =0.65 in both cases

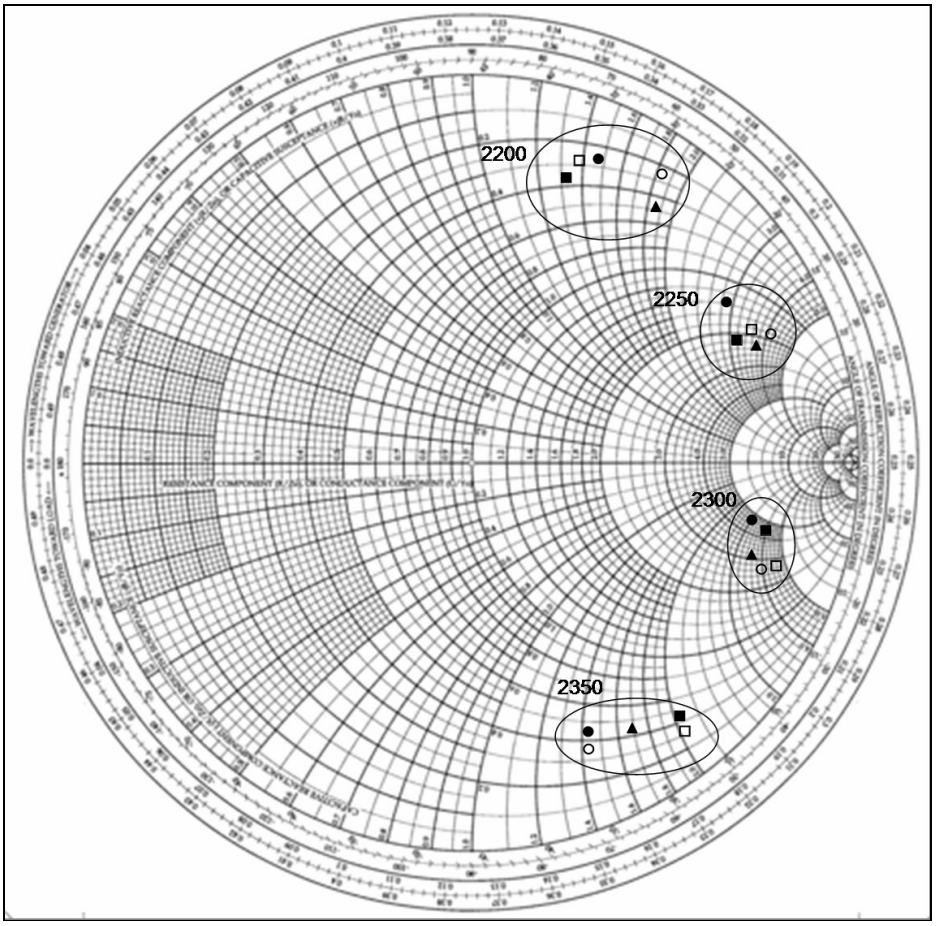

Figure 4.6 – Smith chart plot of input impedance compared with [13]

▲: measured, ■: calculated [13] (S/L_p =0.65), ●: calculated [13] (S/L_p =0.45), □: calculated (S/L_p =0.65), ○: calculated (S/L_p =0.45)

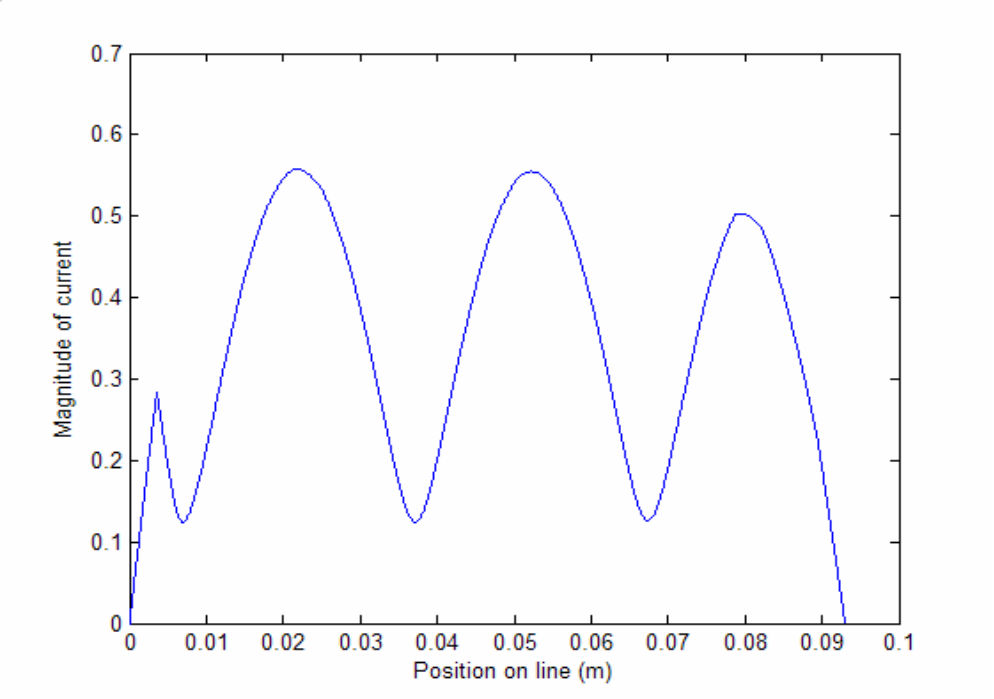

(a)

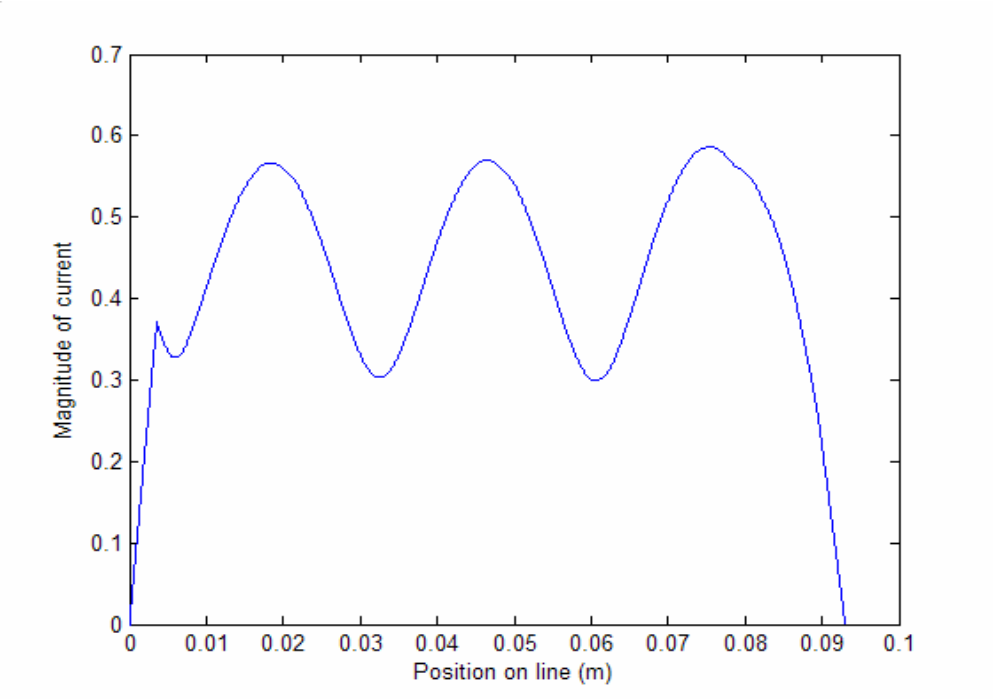

(b)

Figure 4.7 – Magnitude of line current at (a) 3400MHz and (b)3700MHz

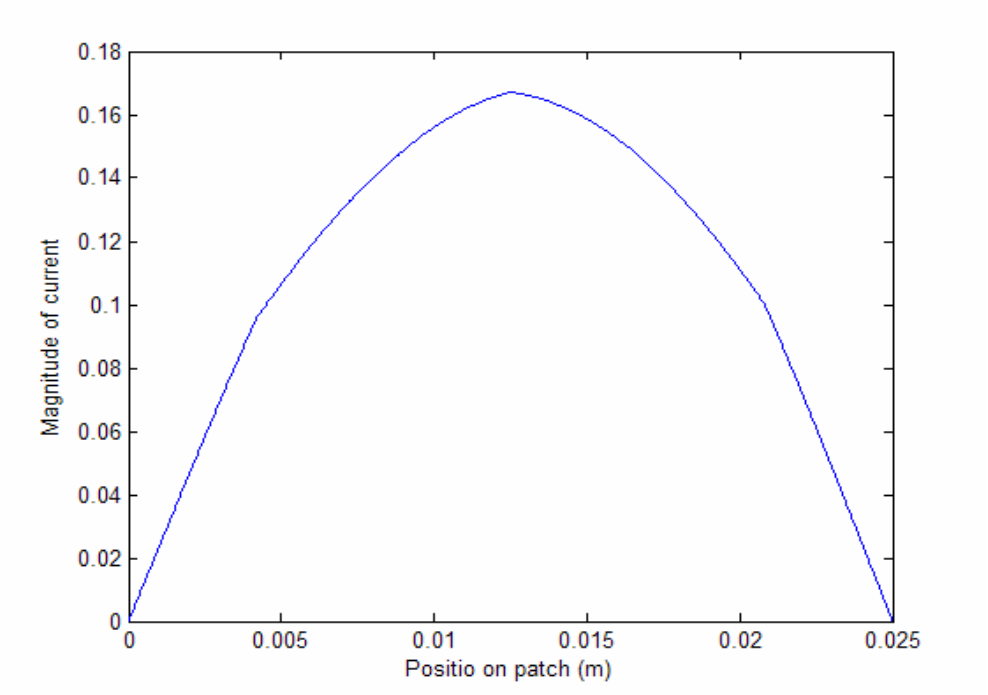

(a)

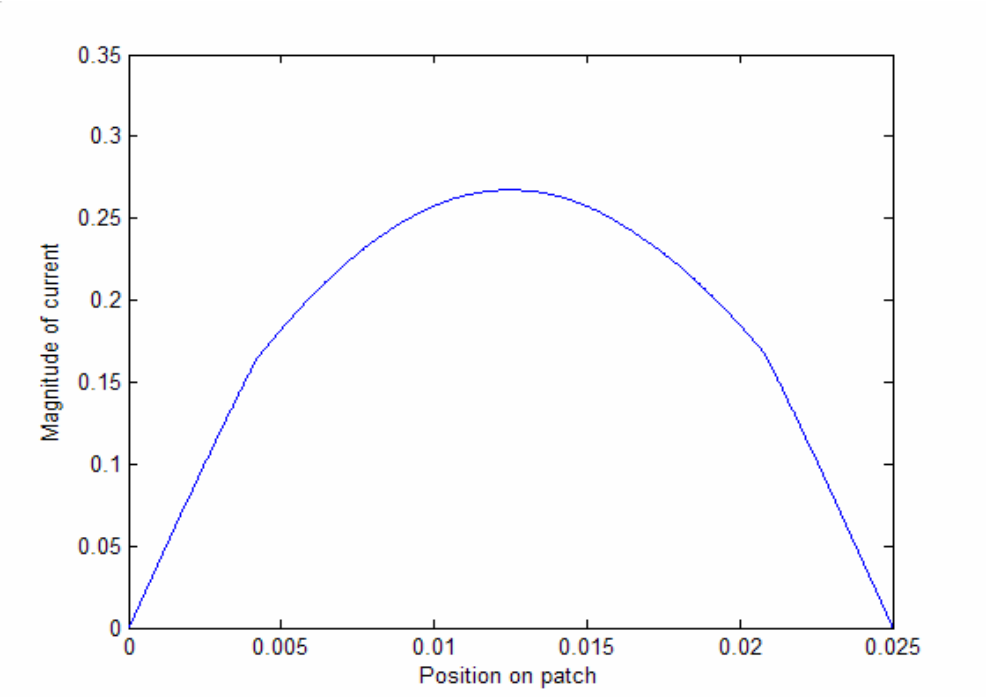

(b)

Figure 4.8 – Magnitude of patch current at (a) 3400MHz and (b)3700MHz

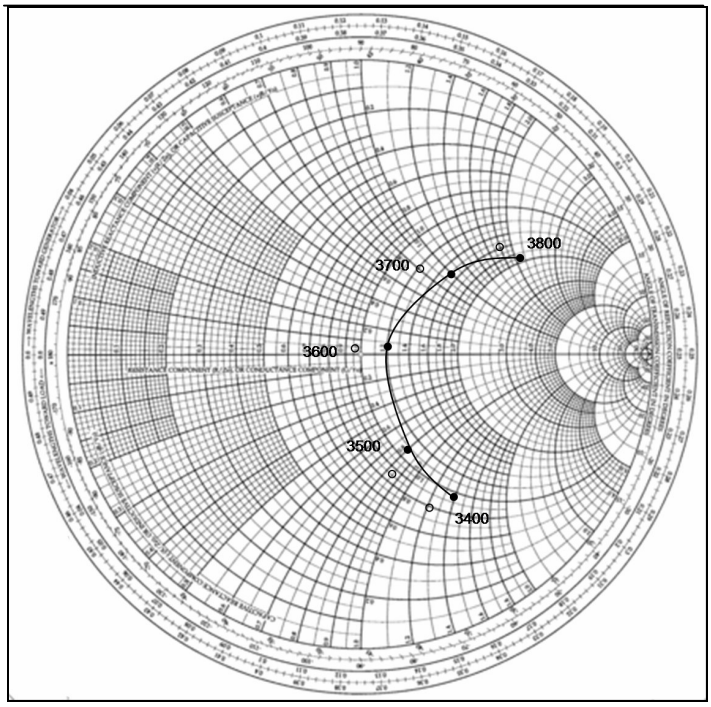

Figure 4.9 – Input impedance of proximity coupled microstrip antenna compared with results given in [13], ●:[13], ○:calculated

CHAPTER 5

CONCLUSION

In this thesis, MoM/spectral domain Green's function formulation is developed for the analysis of planar rectangular microstrip patch antennas with different feed techniques. Formulation for microstripline, microstrip line fed patch, proximity coupled patch and slot coupled patch are given. For all these cases equivalent problems are defined and integral equations are obtained from boundary conditions. Then, MoM is applied to convert these integral equations to a system of linear equations. Currents on the conducting surfaces as well as equivalent magnetic currents on the apertures are modeled as a sum of piecewise sinusoidal sub domain basis functions with unknown coefficients which are calculated by solving the system linear equations. Convergence of numerical calculation of integrals of self and mutual impedance is studied carefully. Furthermore, pole singularity in these integrals is handled properly.

Fortran code is generated to evaluate currents on the lines and patches and input impedance for these structures. Numerical results in the form of line and patch currents and input impedance are calculated by this code and compared with the results available in the literature.

Reflection coefficient of a microstrip line with properties given in [17] is calculated and compared with the ones in [17]. Reflection coefficient values obtained for different width and substrate thickness show good agreement with that of Pozar's paper [17].

Current distributions and the input impedance of microstrip line fed patch antenna structure are calculated by the developed code for different frequencies. Calculated values are compared with the results of [13]. It is observed that results are in good agreement with the ones in [13]. Treatment of feed line in this thesis is different than one in [13].

Proximity coupled microstrip antenna structure is also investigated. Input impedance values evaluated by the developed code are in good agreement with the values given in [13].

Formulation and code modules can easily be extended to analyze different microstrip antenna structure such as stacked patches. As a future work, the code will be modified to analyze arrays of slot coupled patch antennas. For large arrays, when the distance between two elements is larger than few wavelengths, convergence problem is observed for the evaluation of mutual impedance integrals. For such cases, asymptotic evaluation of integrals can be considered.

REFERENCES

[1] Carver, K.R., and Mink, J.W., "*Microstrip Antenna Technology"*, IEEE Trans. Antennas and Propagation, vol. AP-29, pp. 2-24, Jan. 1981

[2] Pozar, D.M., *"Microstrip Antenna Aperture Coupled to a Microstripline"*, Electronic Letters, vol. 21, 2, pp. 49-50, Jan. 1985

[3] Balanis, C.A., *Antenna Theory: Analysis and Design*, *2nd Ed.,* Wiley, Canada, 1997

[4] Ittipiboon, Apisak; Oostlander, Ron; Antar, Yahia M.M. and Cuhaci, Michel, "*A Modal Expansion Method of Analysis and Measurement on Aperture Coupled Microstrip Antenna*", IEEE Trans. Antennas and Propagation, vol. 39, 11, pp. 1567-1574, Nov. 1991

[5] Himdi, M. and Daniel, J.P. and Terret, C., "*Transmission Line Analysis of Aperture-Coupled Microstrip Antenna",* Electronic Letters, vol. 25, 18, pp. 1229-1230, Aug. 1989

[6] Jaisson, D., "*Transmission Line Model for the Input Impedance of a Slot Coupled Rectangular Patch Antenna*", IEE Proc. Microwave. Antennas Propag., vol. 153, 5, pp. 461-468, Oct. 2006

[7] Sullivan, P.L. and Schaubert, D.H., *"Analysis of an Aperture Coupled Microstrip Antenna",* IEEE Trans. Antennas and Propagation, vol. AP-34, pp. 977-985, August 1986

[8] Rathi, Vivek; Kumar, Girish and Ray, K. P., "*Improved Coupling for Microstrip Patch Antennas*", Trans. Antennas and Propagation, vol. 44, 8, pp. 1196-1198, Aug. 1996

[9] Targonski, S. D. and Pozar, D. M., "*Improved Coupling for Aperture Coupled Microstrip Antennas*", Electronic Letters, vol. 27, 13, pp.1129-1131, June 1991

[10] Wang, Youbao; Bo, Yaming and Ben De, "*Wideband Aperture Coupled Microstrip Antenna with Stubs*", CEEM'2006/Dalian, pp 682-684.

[11] Takeuchi, Kazunori; Chujo, Vataru and Fujise, Masayuki, "*Fundamental Characteristics of a Slot Coupled Microstrip Antenna Using High Permittivity Feed Substrate*", European Microwave Conference 1992 22nd, vol.2, pp. 669-774, Oct. 1992

[12] Harrington, R.F. *Field Computation by Moment Methods*, IEEE Press, 1993

[13] Pozar, David M., "*A Rigorous Analysis of a Microstripline Fed Patch Antenna"*, IEEE Trans. Antennas and Propagation, vol. AP-35, 12, pp. 1343-1350, December 1987

[14] Pozar, David M., "*Input Impedance and Mutual Coupling of Rectangular Microstrip Antennas*", IEEE Trans. Antennas and Propagation, vol. AP-30, 6, pp. 1191-1196, November 1982

[15] F.D. Hildebrand, *Introduction to Numerical Analysis,* New york: McGraw-Hill, 1956

[16] Onur, Bakır, *Investigation of Finite Phased Arrays of Printed Antennas on Planar and Cylindrical Grounded Dielectric Slabs,* Bilkent University Thesis, August 2006

[17] Jackson, W. J. and Pozar, D. M. "*Full-Wave Analysis of Microstrip Open End and Gap Discontinuities*", IEEE Trans. Microwave Theory and Techniques, vol. MTT-30, 10, pp. 1036-1042, October 1985